HAL
open science

The last 30,000 to 700,000 years ago: Unravelling the timing of human settlement for the Palaeolithic site of Kozarnika

Maryam Heydari, Guillaume Guérin, Nikolay Sirakov, Philippe Fernandez, Catherine Ferrier, Aleta Guadelli, Jean-Claude Leblanc, Stanimira Taneva, Svoboda Sirakova, Jean-Luc Guadelli

To cite this version:

Maryam Heydari, Guillaume Guérin, Nikolay Sirakov, Philippe Fernandez, Catherine Ferrier, et al.. The last 30,000 to 700,000 years ago: Unravelling the timing of human settlement for the Palaeolithic site of Kozarnika. Quaternary Science Reviews, 2022, 291, pp.107645. 10.1016/j.quascirev.2022.107645 . insu-03751923

HAL Id: insu-03751923

https://insu.hal.science/insu-03751923v1

Submitted on 15 Dec 2022

HAL is a multi-disciplinary open access archive for the deposit and dissemination of scientific research documents, whether they are published or not. The documents may come from teaching and research institutions in France or abroad, or from public or private research centers.

L'archive ouverte pluridisciplinaire **HAL**, est destinée au dépôt et à la diffusion de documents scientifiques de niveau recherche, publiés ou non, émanant des établissements d'enseignement et de recherche français ou étrangers, des laboratoires publics ou privés.

Manuscript File Click here to view linked References

To be submitted to the journal of Quaternary Science Reviews

The last 30,000 to 700,000 years ago: unravelling the timing of human settlement for the Palaeolithic site of Kozarnika

Maryam Heydari[1,2]*, Guillaume Guérin[2,3], Nikolay Sirakov[4], Philippe Fernandez[5], Catherine Ferrier[6], Aleta Guadelli[7], Jean-Claude Leblanc[8], Stanimira Taneva[4], Svoboda Sirakova[4] and Jean-Luc Guadelli[6]

[1]Institute of Earth and Environmental Sciences, University of Freiburg, Albertstr. 23b, 79104 Freiburg, Germany
[2]IRAMAT-CRP2A, UMR 5060, CNRS-Universite Bordeaux Montaigne, Maison de l'archéologie, Esplanade des Antilles, 33607 Pessac cedex, France
[3]Université de Rennes, CNRS, Géosciences Rennes, UMR 6118, 35000 Rennes, France
[4]National Institute of Archaeology with Museum-Bulgarian Academy of Sciences, 2, Saborna Street, 1000 Sofia, Bulgaria
[5]CNRS, Aix Marseille Univ, Minist Culture, LAMPEA UMR 7269, Maison Mediterraneenne des Sciences de l'Homme, 5 Rue du Chateau de l'Horloge BP 647, F13094, Aix-en-Provence, France
[6]PACEA-UMR5199 CNRS, Université de Bordeaux, Allée Geoffroy Saint Hilaire, Bâtiment B18, CS50023, 33615 Pessac Cedex, France
[7]National Institute of Immovable Cultural Heritage, Latchezar Stanchev Street 7, 1125 Sofia, Bulgaria
[8]TRACES-UMR5608 CNRS, Université de Toulouse le Mirail, Maison de La Recherche, 5, Allées Antonio Machado, 31048 Toulouse Cedex 1, France

*Corresponding author: mariheyd@gmail.com

Abstract

Kozarnika cave is a renowned prehistoric site in the Balkans, which contributes significantly to our understanding of the human past due to its rich assemblages associated with the Lower to Upper palaeolithic periods. To unravel the timing of human occupations in Kozarnika, various dating methods have been employed in the past. Radiocarbon dating was used to unfold the timeframe for the Kozarnikian lithic tradition uncovered in the Upper Palaeolithic sequence of the cave, and paleomagnetic dating assigned the Brunhes–Matuyama reversal to the layer beneath the Lower Palaeolithic assemblages.

In this study, we employed luminescence-dating methods including a body of different signals to date sediment layers from the top to the bottom of the sequence covering the period of ca 30 to 700 ka. Our investigations revealed that the Kozarnikian tradition in layers 5a-c falls between 30–35 ka. Following that, we suggest that the Middle Palaeolithic period initiated between 250–309 ka and lasted until 40–53 ka. More importantly, we have updated the age of the Neanderthal radius discovered in the Mousterian assemblages to 201±17 ka.

Our dating of the Lower Palaeolithic assemblages in the cave rendered the period of ca 300-700 ka. Taking into account the timeframe suggested by the paleomagnetic sequence <780 ka it is likely that we have reached the threshold of the luminescence dating method and the age range may represent the minimum age for this period.

1. Introduction

The Balkans are renowned for witnessing different hominin and human species of inhabitants due to the location between the Near East and the Western Europe during the long period of the Palaeolithic. Human remains associated with the Neanderthals or anatomically modern humans (AMH) have been discovered in the Middle and Upper palaeolithic assemblages in various sites (e.g., Galanidou, 2004; Glen and Kaczanowski, 1982; Hoffecker, 2009; Hublin et al., 2020; Strait et al., 2016; Tillier et al., 2017). Additionally, the high possibility of interaction between two human species (Fu et al., 2015; Hajdinjak et al., 2021) renders this region unique for further investigations.

Establishing a reliable temporal framework disclosing the timing of hominin species' settlements, the demise of one (e.g., Neanderthal), and domination of another (e.g., AMH) is a fundamental study, and it can be revealed through applying numerical dating methods. Among the whole body of techniques, radiocarbon dating plays a major role to track dynamics of the human peopling during the Late Middle to Upper Palaeolithic periods generally for Europe (e.g., Higham et al., 2014) and in particular for the Balkans (e.g., Alex et al., 2019; Devièse et al., 2017; Fewlass et al., 2020; Higham et al., 2006.; Trinkaus et al., 2003).

Whilst numerous temporal frameworks have been constructed to date the humans' fossils or the artefacts attributed to the Middle/Upper Palaeolithic, the number of available datasets is relatively scarce for the Lower to Middle Palaeolithic. This could be explained due to the shortage of the well-preserved Lower Palaeolithic sequences in eastern Europe (Doronichev, 2008). Having said that, the Palaeolithic site of Kozarnika has been a special place all along not only because of its rich archaeological remains related to the Lower Palaeolithic but also for offering the first Bulgarian Neanderthal's remain, a radius associated with a rich Mousterian assemblage (Tillier et al., 2017). Furthermore, the Upper palaeolithic industry found in the cave stands out from the other lithic productions and is known as *Kozarnikian* (Guadelli et al., 2005; Tsanova, 2006; Sirakov et al., 2007).

During the last decades, different dating methods have been employed to establish reliable chronologies for the sequences in the cave. The Upper Palaeolithic sequence was dated using the radiocarbon method (Guadelli et al., 2005, in press). Moreover, preliminary luminescence

ages attributed to the neanderthal radius were previously published (Tillier et al., 2017). In another study, a palaeomagnetism sequence was established for stratified layers in Kozarnika (Muttoni et al., 2017). Finally, a timeframe for the Lower and Middle Palaeolithic assemblages was demonstrated on mammal biochronology (Guadelli et al., 2005, in press; Fernandez and Cregut-Bonnoure, 2007; Popov and Marinska, 2007; Sirakov et al., 2010).

In this study, we applied multiple luminescence-dating methods not only to elucidate the timeframe of humans resided during the Middle and Upper Palaeolithic but to shed light on the timing of the inhabitants at the Lower Palaeolithic and provide a full chronology covering the complete sequence through sediment samples. This will allow us to improve our understanding about the timing of humans' settlements, particularly for Kozarnika and more widely for the Balkans.

1.1 Site location

Kozarnika cave is located in the northwest of Bulgaria, 30 km away from the Serbian border (Fig. 1). The site is situated in the northern slopes of the Balkan Mountains, merging to the Danubian Plain, which is extended to the Danube River to the north. The cave is positioned at an altitude of 481 m on the mountainside of Bashovishka Bara valley. The streams in the valley drain into the Skomlia River irrigating the region, which feeds the Danube River ca 30 km away.

The first report about Kozarnika dates back to 1933 (Popov (Попов), 1933) and years after in 1996, the site was excavated systematically by Bulgarian-French researchers (Guadelli et al., 2005). Following years of collaborative work, 21 geological layers were discovered in a sequence of about 9 m containing assemblages attributed to the Lower, Middle, Upper Palaeolithic as well as Holocene.

Fig. 1.

1.2 Stratified geological layers including archaeological discoveries

The Bashovishka Bara valley has cut 185 m deep into the northern foothills of the Balkan through three main geological formations. The top formation belongs to the Early Jurassic which at the middle is replaced by the Middle Jurassic and finally at the bottom is superimposed on the Late Jurassic. The Kozarnika cave consists mainly of limestone, which is formed in the Upper Jurassic geological formation (Guadelli et al., 2005; Sirakov et al., 2010). The cave is part of a larger karst landscape with other caves discovered in the north-western region of Bulgaria.

The Pleistocene layers in the cave are generally well-preserved. However, we observed truncations in the cave for some layers containing Middle and Upper Palaeolithic assemblages (Guadelli et al., 2005; Sirakov et al., 2010). These truncations are likely stemming from the cave's subsequent use in modern times, when it was used as a mushroom farm and goat farm, and finally as a bunker in the 1960s.

The geological layers in the cave were categorised into four main groups covering the top to the bottom of the excavation profile (Fig. 2). Their general characteristics are explained below.

Fig. 2.

1.3 Geological layers containing the archaeological finds

Layers 3a-4. These layers with a thickness of 1 m to 1.4 m form the top of the sequence. Most of the sediment is of aeolian origin. Nevertheless, a considerable amount of calcareous clasts gravels in colours from light brown to whitish silty medium can be found in this part in addition to debris from the ceiling and the walls of the cave. The archaeological assemblages belong to the middle and late Kozarnikian tradition (the indigenous eponymous bladelets industry mentioned above) associated with the Upper Palaeolithic (Guadelli et al., 2005).

Layer 5a-10a. These layers show thicknesses of 1.2-1.5 m and were deposited through a combination of aeolian transport (recognised by beige silty-fine grains), and sediment fragments from the ceiling and walls (identified with coarse grains and calcareous gravel and pebble). Both groups of sediments are distributed irregularly over the section. Layer 5b contains some volcanic ashes superimposed on layers 6 and 7, which both were composed of silty sediment varying from light grey (6) to light brown (7). Due to the similarity between the origin of these two layers, they both were considered as one layer named 6/7. The calcareous gravels and charcoal also were sparsely observed in this layer (Ferrier et al., 2009). Generally speaking, the formation of layers 5a, 6/7, and 10a is dominated by aeolian processes. Layers 10a-9a contain archaeological elements related to the Middle Palaeolithic period. The archaeological finds in layer 6/7 are consistent with the Middle and Initial Upper Palaeolithic assemblages. The upper layer (5a) contains the blade industry known as the Kozarnikian tradition.

Layer 10b-10c. These layers originated from roughly weathered calcareous gravel and pebbles, with a combination of loamy sand with dark brown colour that could be attributed to human activity in the past. The sediment thicknesses of these layers vary from 15 cm to 50 cm

and contain archaeological artefacts associated with the very early Middle Palaeolithic with the Mousterian characteristics.

Layer 11a-13. These layers were located at the bottom of the sequence having a thickness of ca 2.5 m. The sediments in this section consist of orange loamy fine and coarse fractions with flint, limestone, and debris from the ceiling and the walls of the cave. In particular calcareous pebbles and blocks with various concentrations were observed in layer11a as a common feature of this layer in a different part of the cave. The same pattern with a combination of a dark fraction of silty material with quartz origin applies for layers 11b, 11c, 12, and 13. It is likely that this sequence of layers is a result of mudslides according to Ferrier et al. (2009). All of these layers comprise findings from an industry affiliated with the Lower Palaeolithic period.

2. Material and Methods

Luminescence dating estimates energy (radiation dose) deposited in natural minerals after the last sunlight exposure. This quantity is known as the equivalent dose (estimated in the laboratory), which is built up by energy emitted by natural radioelements in the sediment over the burial time (dose rate). Dividing the equivalent dose by the corresponding dose rate, results in the burial time (age). We used various techniques to determine the equivalent doses of the samples. First, we began with the blue optically stimulated luminescence (OSL) for quartz (Huntley et al., 1985), followed by post infrared stimulated luminescence at the elevated temperature (Post-IR IRSL, Thomsen et al., 2008) to completely cover the Middle to the Upper palaeolithic sequences. In addition, the infrared stimulated luminescence (IRSL, Hütt et al., 1988) signals for some samples were measured at 50 ˚C to crosscheck with the two other age series.

It is well-known that signal saturation is a key parameter hampering the application of luminescence dating for the Lower to Middle Palaeolithic. Given that, we attempted to tackle this problem by combining various luminescence signals with different saturation degrees to extend the age limit. We switched to violet stimulated luminescence (VSL) (Ankjærgaard et al., 2016, 2013; Jain, 2009) on quartz accompanied by infrared radiofluorescence (IR-RF) (Trautmann et al., 1999b, 1999a, 1998, for review see Murari et al., 2021) on K-feldspar to estimate ages for the older samples.

The dose rates were estimated by means of both *in situ* and laboratory measurements for all samples (further details below).

2.1 Sample preparation

We present ages for 18 sediment samples extracted from the profile, using opaque tubes (see Table 1). Our sample preparation followed routine procedures applied in luminescence dating (Preusser et al., 2008). After conducting the grain size analysis (see Fig. S1 in the supplementary material) coarse grains with 180 µm to 250 µm diameters were extracted using wet sieving. To eliminate carbonates, the obtained fraction of sediments was rinsed in HCl (30%) over a couple of hours until no further reaction was observed. Following that, they were soaked in H_2O_2 (30%) to remove organic compounds. Later, density separation was carried out through lithium hetero-polytungstates (LST) heavy-liquid. First, quartz grains were separated from the bulk sample using a density of 2.62 g cm^{-3}. Then, K-feldspar grains were extracted from the remaining material by applying the LST with a density of 2.58 g cm^{-3}. We removed the outer layers of quartz and K-feldspar grains affected by alpha particles by etching them with HF; (40% for 40 min on quartz and 10% for 10 min on K-feldspar). Etching was followed by resting the grains in HCl (15%) overnight to eliminate unwanted fluorides. Finally, all grains were sieved for the second time with the smaller mesh size (<180 µm) to remove any remaining fragmented grains.

Table 1

2.3 Instrumentation

Various instruments were employed for measuring luminescence signals using different minerals and techniques. Blue OSL was measured on Freiberg Instrument lexsyg SMART TL/OSL systems (Richter et al., 2015) equipped with five blue LEDs (458 Δ 3 nm, max. 100 mW cm^{-2}) and five infrared LEDs (850 Δ 3 nm, max. 300 mW cm^{-2}) as well as on a Freiberg Instrument lexsyg research reader (hereafter L1,(Richter et al., 2013) equipped with five blue LEDs (458 Δ 10 nm, max. 100 mW cm^{-2}) and five infrared LEDs (850 Δ 3 nm, maximum 300 mW cm^{-2}). The stimulation powers for lexsyg research and lexsyg SMART systems were set to 100 $mWcm^{-2}$ and 40 $mWcm^{-2}$, respectively. Signals were detected using a UV filter combination (Hoya U340, 2.5 mm and Delta BP 365/50 EX) in both systems.

Post-IR IRSL ($pIR_{50}IRSL_{290}$) signal was measured using a blue-violet filter combination Schott BG 39 (3 mm) and Chroma D410/30x in Freiberg Instruments lexsyg research reader with a stimulation power of 100 $mWcm^{-2}$.

IRSL signals were measured using Risø TL/OSL DA-15 and DA-20 readers equipped with five blue LEDs (470 Δ 20 nm, max. 105 mW cm^{-2}) and five infrared LEDs (870 Δ 40 nm, max. 145 mW cm^{-2}). Signals were detected through a combination of Schott BG39 and Corning 7-59 (Bøtter-Jensen et al., 2003).

VSL signals were measured using Freiberg Instruments lexsyg research reader containing violet-emitting LEDs (405 Δ 3nm, max. 100 mW cm^{-2}). The stimulation power was set to 100 $mWcm^{-2}$ and the signal was detected using a combination of a Hoya U340 (2.5 mm) and an AHF-BL HC 340/26 interference filter.

All systems were operated with a $^{90}Sr/^{90}Y$- source which was calibrated using Risø calibration quartz (Hansen et al., 2015). The dose rates available for each sample in lexsyg research and SMART as well as Risø TL/OSL systems were ca 8 Gy min^{-1}, 11 $Gymin^{-1}$, and 7 Gy min^{-1} at the measurement dates, respectively.

IR-RF was measured through another Freiberg Instrument lexsyg research system, which was equipped with a Hamamatsu H7421-50 PMT in conjunction with a Chroma D850/40 interference filter. A calibrated $^{90}Sr/^{90}Y$- source delivered a dose rate of ca 3 Gy min^{-1}. For the bleaching of the natural IR-RF, we used the internal solar simulator of the machine. All samples were prepared using stainless steel cups with a diameter of 8 mm.

Approximately, a hundred grains were mounted in diameter of 3 mm using silicon oil for measuring blue OSL, $pIR_{50}IRSL_{290}$, and IRSL. The number of grains was increased for VSL and IR-RF; in these cases, the cups were fully covered by grains, representing several thousand grains.

2.4 Dose rate

The dose rate available to quartz and feldspar consists of external and internal parts due to the activity of the radioelements outside and inside of the grains. For the external part, we have only estimated beta and gamma dose rates because the etching removed the outer layer of the grains affected by alpha-radiation.

We estimated the radionuclide concentrations of U, Th, and K using high-resolution low background gamma-ray spectrometry (Guibert and Schvoerer, 1991). The obtained concentrations were then turned into beta-dose rates using conversion factors after Guérin et al. (2011) and corrected using grain size attenuation factors following Guérin et al. (2012). The effect of water on dose rate was corrected after Nathan and Mauz (2008). We estimated the saturation water content based on the grain size distribution as suggested in Nelson and Rittenour (2015). The sample-specific percentages of the sand, silt, and clay fraction are displayed in Table S1 in the supplementary material. We have used the fraction of 0.5±0.2 (of the saturation value) as a representative value to approximate the past water content. We increased the obtained value to 20±8% for samples (Koz16 to Koz21) due to the mudflow origin of layer 11b downwards.

Gamma-dose rates were estimated using artificial dosimeters (Al_2O_3:C chips; see Kreutzer et al., 2018 for further details) for all samples. The chips were first heated up for 10 min at 350° C. Three chips were inserted in each aluminium tube and remained in the sediment for 271 days. After retrieving, the stored energy was measured using Daybreak 2200 OSL reader system (Bortolot, 2000). The chips were stimulated through green light (Nichia NSPG10) and the emissions were recorded through a 7.5 mm Hoya U-340 filter. For comparison, the gamma-dose rate was also estimated using radioelement concentrations derived from the gamma-ray spectrometry. The concentrations were converted to the dose rate after convention factors tabulated in (Guérin et al., 2011) and corrected for water content following (Guérin and Mercier, 2012).

The cosmic-dose rate was calculated using the coordinate of the site and the overburden depth after the procedure in Prescott and Hutton, 1994; Prescott and Stephan (1982). The uncertainty of the cosmic dose rate was estimated at 10% after Prescott and Hutton (1994).

The internal dose rate was estimated using K and Rb concentrations of 12.5±0.5% (Huntley and Baril, 1997) and 460±20 ppm after Mejdahl (1987) respectively. The internal dose rate for quartz coarse grains was taken from Mejdahl (1987).

2.5 Luminescence signal measurements

We applied several protocols to both quartz and feldspar grains and accordingly the corresponding signals were used for dating. We have measured blue-OSL and VSL for quartz grains. In addition, IRSL at 50°C, and $pIR_{50}IRSL_{290}$ at an elevated temperature (290 °C) were measured to establish ages based on feldspar grains. Nevertheless, this approach potentially could disclose the history of grains' bleaching, which is a worthy matter of consideration since the accuracy of the obtained ages heavily depends on it. Below, the setting for each protocol is explained.

<u>Blue optically stimulated luminescence (blue-OSL)</u>

We used the single aliquot regenerative (SAR) dose protocol (Murray and Wintle, 2000) to estimate the equivalent dose (D_e) for each sample.

First, the dominance of the fast-decaying signal favourable for relatively young sediment samples was tested. We simply compared the blue-OSL signal from one of Kozarnika's samples with calibrated quartz Risø batch 90 (Hansen et al., 2015), which is known to be dominated by the fast decaying luminescence signal. In addition, a linearly modulated OSL (LM-OSL, Bulur, 1996) technique was applied to deconvolute the signal components for this sample to be compared with the calibration quartz. D_e estimation was carried out using Analyst

software v. 4.53 (Duller, 2015). A single saturating exponential function was used for fitting the dose-response curve.

The regenerative dose steps were followed by a null dose delivered to monitor charge transfers. This step was followed by a repetition of the first regenerative dose to verify significant sensitivity changes. In the end, the same dose as the first regenerative was delivered to the samples and the corresponding signal was measured after stimulating with IRSL followed with blue OSL to check any significant contamination by feldspar grains after Duller (2003).

The luminescence signal was measured at 125°C for 40 s after preheating at 260°C for 10 s. The preheat plateau test was applied to sample Koz2 to select an appropriate temperature before measuring the signal in SAR protocol (Murray and Wintle, 2000). In this test, D_es were measured at various degrees starting from 200°C and reaching 300°C (ramping up by 20°C at each step). The cut heat was 40°C lower than the corresponding preheat temperature. Dose-recovery tests were conducted on some samples to monitor the reliability of the SAR protocol's parameters. Samples were bleached for 100 s using blue light, followed by a pause of 10,000 s. For the second time samples were bleached using blue light and then they received a beta dose inside the OSL reader approximately equivalent to their natural doses (Koz2, 4, 7, 10).

Infrared stimulated luminescence ($IRSL_{50}$ and $pIR_{50}IRSL_{290}$)

K-feldspars were used for estimating the D_es for some of the samples to obtain independent ages, also revealing the grains' bleaching histories. Particularly, K-feldspar is favourable when the expected temporal range is higher than what the blue-OSL signal of quartz can achieve. Due to this higher upper age limit, this mineral has been used to unravel the temporal frameworks attributed to the Middle and also Lower Palaeolithic periods of the cave. Having said that, the drawback of using feldspar is athermal anomalous fading (loss of signal over time (Wintle, 1973)) that impedes the proper estimation of the true D_e. To overcome this problem, we determined the fading rate (Huntley and Lamothe, 2001) and corrected its effect on D_e. In this study, for three samples Koz4, Koz8, and Koz11, IRSL signals were measured (six aliquots for each sample) following fading measurement after a pause of approximately 1 h and 4 h. The fading rate was calculated using the function *Luminescence::analyse_FadingMeasurement()* implemented in the R (R Core Team, 2021) 'Luminescence' (Kreutzer et al., 2012; Kreutzer et al., 2021) package after methodological work by (Huntley, 2006). These values were then used to correct the D_e estimates using *Luminescence::calc_Huntley2006()* after Kars et al., 2008 and King et al., 2018 also embedded in the R 'Luminescence' package. A single saturating exponential function was used to generate a dose-response curve.

Furthermore, we measured the IRSL signal at an elevated temperature following the IRSL at 50°C. This method was suggested after (Buylaert et al., 2011; Li and Li, 2011; Thiel et al., 2011; Thomsen et al., 2011, 2008) and it is proposed that the signals do not suffer from the fading, or at least the fading rate can be considered as insignificant (Buylaert et al., 2012, 2011). The parameters' setting for measuring this signal was derived from Buylaert et al., (2012) and was applied to a large number of samples containing 4 to 12 aliquots.

Infrared radiofluorescence (IR-RF)

Aside from the IRSL signal, K-feldspar emits another signal during ionising radiation, which is detected in the infrared wavelength range, known as IR-RF (for a recent review see Murari et al., 2021). The advantage of employing this signal is the larger age limit, which presumably could cover the temporal range attributed to the Lower Palaeolithic sequence of the cave. For IR-RF measurements, we have employed the parameters' setting suggested by Frouin et al. (2017). The regenerative signals were measured after bleaching of ca 3 h (10,800s). To ensure this time sufficiently reset the natural IR-RF signal, we also carried out a bleaching test.

The D_es for samples Koz11, Koz14, Koz16, Koz18, Koz20, and Koz21 were estimated through the approach of horizontal and vertical sliding (Kreutzer et al., 2017; Murari et al., 2018) implemented in *Luminescence::analyse_IRSAR.RF()*.

Violet stimulated luminescence (VSL)

Unlike the relatively early saturation of the fast decaying blue-stimulated luminescence signal, some slow decaying components in quartz are deemed to be of higher saturation dose (Jain, 2009). This makes them attractive for dating older sediment like the Lower Palaeolithic sequences. Thus, we have applied the SAR protocol suggested by Ankjærgaard et al., (2016) to estimate the D_e based on deep traps. This protocol was designed in a way that first the fast-decaying component is depleted using blue light stimulation and violet stimulation is then applied to probe the slow decaying signal with a higher saturation dose. We tested this technique on several samples (Koz8, 14, 16, 18, 21). However, the outcome of this application was not promising (all signals were in apparent saturation), therefore, we proceeded with the multiple aliquot additive dose (MAAD) protocol as an alternative solution to the standard SAR protocol offered in (Ankjærgaard et al., 2016). We used one of the youngest samples (Koz4) for which an independent age using the blue OSL technique was estimated and for which we had enough grains available to prepare a large number of aliquots.

The prepared samples were categorised into several fractions (each group comprising six aliquots) which were exposed to various amounts of beta irradiations on top of the natural dose. The first irradiative dose was set to 117 Gy and gradually it was increased to the dose of 2760

Gy. In the next step, following the approach of Ankjærgaard et al. (2016) we measured only the natural luminescence signal (L_n) which was corrected by the test dose signal (T_n) for each set of irradiated samples to minimise the impact of sensitivity change arising from repeated irritations and heating of the samples. Then the obtained L/T values were subsequently used to construct the MAAD dose-response curve fitted using a Lambert W function (Pagonis et al., 2020). Afterwards, the L_n/T_n ratios measured from the natural samples were used (six aliquots for each natural sample) to estimate the D_es (see result section).

3. Results

3.1 Dose rate

Table 2 shows the obtained concentrations of U, Th, and K. The equivalent U concentration was determined from the top (pre-^{226}Ra) and the bottom of the chain (post-^{226}Ra). This allows checking potential disequilibria in the U chain (Guibert et al., 2009). For samples Koz6, Koz7, Koz18, radioactive disequilibria were observed. To minimise this effect on the dose rates, instead of using the obtained values from the bottom of the chains (which were smaller than the top vaules), the average of the top and bottom concentrations was calculated and employed to estimate the dose rates for those samples (Table 3).

Table 2

The beta-dose rate for all samples ranged from 0.86±0.04 Gy/ka to 1.70±0.08 Gy/ka. The *in situ* and laboratory (i.e. from the concentrations of K, U and Th) gamma-dose rates ranged from 0.19± (<0.01) Gy/ka to 0.72±0.01 Gy/ka and from 0.49±0.02 Gy/ka to 0.97±0.03 Gy/ka, respectively. We have illustrated the two distinct series of gamma dose rates in Fig. 3. As shown in this figure, most *in situ* gamma-dose rates were significantly smaller than the corresponding gamma-dose rates obtained through means of gamma-ray spectrometry. It should be noted that we did not have a reliable estimation of the water content at sampling data, thus, it is likely that our estimation of the past water contents (varying between 14±6% to 20±8 %) is not in close alignment with the current water content. However, this does not explain the substantial discrepancies observed between the two dose rate results. It is more likely that the limestone pebbles and gravels that can readily identify in Fig. 2 caused a heterogeneous environment in which the *in situ* gamma dose rate values are smaller than the laboratory measurements. Therefore, we considered the *in situ* values more representative of the gamma dose rates received by the samples and used those values to determine the final dose rate. Particularly, because they cover gamma rays from larger distances and hence provide more

accurate estimates. The internal dose rate for quartz was set to 0.06±0.03 Gy/ka and a value of 0.90±0.14 Gy/ka was obtained for K-feldspar. Cosmic dose rates varied between 0.06±0.01 Gy/ka to 0.09±0.01 Gy/ka. In the end, the final dose rate for quartz and K-feldspar grains vary between 1.21±0.05 Gy/ka and 2.38±0.09 Gy/ka, and between 2.05±0.15 Gy/ka and 3.22±0.16 Gy/ka, respectively.

Table 3

Fig. 3.

3.2 Equivalent dose (D_e) determination

Blue-OSL

Fig. S2 in the supplementary material illustrates with pseudo-LM OSL (Bos and Wallinga, 2012) the presence of a fast-decaying signal at the beginning of the curve, but it also highlights at least contamination with another signal, at the end of the curve. Fig. S3 (true LM-OSL) revealed that presumably, the slow decaying signals (slow components) are also contributed to the luminescence signal.

We employed late background subtraction; the signal was measured using channels 1 to 3 (0.3 s) and the background was set to 300 to 399 (10 s). The recycling ratios, (a representative value for expressing the sensitivity change after administrating the cycles of heating and irradiating) were within 20% of the unity for all samples. Furthermore, the recuperation signal ratio following the received zero dose was less than 5%. An IR depletion ratio test Duller (2003) was carried out at the end of the SAR protocol and the results were within 10% for all samples. Fig. S4 in the supplementary material depicts the outcome of the preheat test for sample Koz2. We considered 260 ° C and 220° C as acceptable temperatures for the preheat and cut-heat in our SAR protocol; using such elevated temperatures allows subtracting a late background by removing less stable components than the fast component (Jain et al., 2003). Dose recovery ratios for samples Koz2, Koz4 (given dose ca 48 Gy), Koz7 and Koz10 (given dose ca 83 Gy) resulted in 1.02±0.04, 1.01±0.03, 0.96±0.08, 0.91± 0.07, respectively. These values are consistent with 1 within uncertainties and fulfil the standard criterion (commonly accepted is within 10% of unity), indicating the suitability of the SAR protocol's parameters for our samples. However, the smooth reduction in these values alongside increasing the D_es, indicates that reaching the non-linear part of the dose-response curve and may give rise to D_e underestimation.

Fig. 4a and Fig. 5a show typical dose-response curves, and a visual representation of the D_e distribution for sample Koz4 as an example. We have estimated the central dose for each

sample using the arithmetic average (as suggested for multi-grain OSL by (Guérin et al., 2017)), and its uncertainty was determined through the standard error of the mean. The estimated central doses ranged from 48±2 Gy to 117±9 Gy for samples Koz1 to Koz10 (see Table 4). We also measured blue OSL signals for subsequent samples, however, since we reached the saturation limit of the signal, further results were considered untrustworthy or at least underestimated.

$IRSL_{50}$ and $pIR_{50}IRSL_{290}$

$IRSL_{50}$ signals for three samples were measured by integrating the first 6 s and subtracting the last 56 s as the background. The obtained *g*-values (measured for six aliquots per sample) for samples Koz4, Koz8 and Koz11 resulted in 3.25±0.04 (3.52±0.04, norm. 2 days) %/decade, 3.31±0.04 (3.58±0.04, norm. 2 days) %/decade, 3.35±0.07 (3.63±0.07, norm. 2 days) %/decade (see Fig S5). The fading corrected D_es for these three samples were 109±1 Gy, 171±4 Gy, 512±72 Gy, respectively. The typical dose-response curves and D_e distribution for sample Koz4 are illustrated in Fig. 4c and Fig. 5c, respectively.

The $pIR_{50}IRSL_{290}$ signals were measured using the first 8 s and the background was subtracted using the last 60 s of the shine-down curves. The recycling ratios were within 10% of unity and recuperation ratios were less than 5%. The dose-response curves and the D_e distribution for sample Koz4 are depicted in Fig. 4b and Fig. 5b, respectively. The D_e representing the central equivalent dose for all samples was determined using the arithmetic average of D_e values and its uncertainty was estimated using the standard error of the mean. The obtained D_es for our samples varied between 95±3 (Koz2) to 671±36 Gy (Koz14) (see Table 4). Due to the lack of K-feldspar grains for Koz15, we could not measure any signal, however, for the subsequent samples, the corresponding signals were mainly in or close to saturation and thus the outcome was not considered trustworthy.

Fig. 4.

Fig. 5.

Infrared-radiofluorescence (IR-RF)

The result of the bleaching test on sample Koz11 is displayed in Fig. S6. This figure shows that a bleaching time of 10,800 s appears to be sufficient, lying within the plateau. The IR-RF signal was measured using a channel resolution of 10 s. The observed scatter in the points after reaching the plateau is probably induced by negligible movement of grains on the sample

carrier. Typical IR-RF signals for samples Koz11, Koz18, Koz21 are shown in Fig. 6. The natural and regenerative signals are illustrated with red and green, respectively. The horizontal and vertical sliding method was successfully applied to natural signal and an excellent match between natural signal and regenerative is observed. The D_e distributions for samples Koz11, Koz18, and Koz21 are represented in Fig. 7 using kernel density estimate (KDE) plot. The D_e representing the central equivalent dose for each sample is estimated using the arithmetic average and its uncertainty was determined using the standard deviation.

Fig. 6.

Fig. 7.

Violet stimulated luminescence (VSL)

A typical dose-response curve alongside the natural and regenerative signals observed after applying the VSL (SAR) protocol is shown in Fig. S7 for one sample. Fig. S8 shows a smooth increase in the obtained L_n/T_n values as samples' depths are increased along with the profile. This gradual rise suggested that VSL has the potential to yield chronological information, as was already observed in (Ankjærgaard et al., 2016). Fig. 8 illustrates the L/T distribution obtained for each set of six aliquots prepared originally from Koz4; while the first set corresponds to the natural dose, all other sets were irradiated in the laboratory with increasing doses on top of the natural. We tested several fitting functions on our data set. Finally, as depicted in Fig. 8, we fitted a dose-response curve using a Lambert W function to our dataset, which seems to be more justified than other commonly fitting dose-response curve functions (Pagonis et al., 2020). Subsequently, the L_n/T_n obtained from the natural samples were projected onto the fitted curve (Fig. S9). Because of the nature of the MAAD approach, which adds doses on a natural sample that already has a dose, the dose-response curve necessarily intersects with the y-axis. Theoretically, one could attempt to estimate the equivalent dose for the first sample from the intersection of the curve with the x-axis. Due to the exponential character of the curve, this extrapolation comes at the cost of very large uncertainties; hence it was not used here. However, the L_n/T_n signal of Koz4 project onto the MAAD dose-response curve should result in an equivalent dose around 0. We estimated a value of 11±12 Gy for this sample, which is consistent with the zero dose within uncertainty. To estimate the equivalent dose of all other samples, the natural equivalent dose of sample Koz4 based on quartz blue OSL was added to all estimated results to determine the final D_e for each sample.

Fig. 8.

3.3 Age estimation

The obtained ages based on the various signals are presented in Table 4. The OSL dating for the uppermost sample (Koz1) belonging to layer 5a, exhibited an age of 32±2 ka (one sigma). Gradually, the OSL ages increase smoothly with depth until layer 10b (sample Koz11), for which two aliquots out of ten were in saturation. Thus, we considered this age (141±12 ka) to be a minimum age. The corresponding ages for samples Koz11 and Koz12 estimated based on $pIR_{50}IRSL_{290}$ signals led to 161±13 ka and 199±12 ka (one sigma). Subsequently, only the OSL age for layer 10a (59±4 ka) and younger samples above were considered reliable (Fig. 9).

As shown in Fig. 9 (inset) (between layer 5a to layer 10a), the $pIR_{50}IRSL_{290}$ ages were determined for a number of samples. Generally, at first glance, it can be concluded that the $pIR_{50}IRSL_{290}$ ages are older than the corresponding OSL ones. However, apart from one sample (Koz2 from layer 5b), for which no overlapping between the OSL and $pIR_{50}IRSL_{290}$ ages is observed within two sigma (26-33 ka for OSL and 35-43 ka for $pIR_{50}IRSL_{290}$), the rest overlap and the age outcome from the two approaches can be generally evaluated consistently.

The IRSL ages which were fading-corrected were estimated for three samples. All of them are older compared to both, OSL and $pIR_{50}IRSL_{290}$ ages. The obtained IRSL ages resulted in 45±3 ka and 66±4 ka, respectively, for samples Koz4 (layer 6/7) and Koz8 (layer 9c). At 95% confidence, these two ages exhibit timeframes of 39-51 ka and 58-75 ka that overall are in alignment with the periods of 33-41 ka and 48-74 ka ascertained from $pIR_{50}IRSL_{290}$. Nevertheless, the IRSL age of sample Koz11 (layer 10b) 250±40 ka is significantly larger than the corresponding $pIR_{50}IRSL_{290}$ age of 161±13 ka. The IR-RF age for this sample resulted in 201±17 ka; thus, it seems that the $pIR_{50}IRSL_{290}$ age for this sample could be underestimated. The $pIR_{50}IRSL_{290}$ ages increase in depth up to layer 10c. Afterwards, we have a clear indication of signal saturation (four aliquots out of six) for sample Koz16 (layer 11b). From this layer down to the lowermost layer, only IR-RF and VSL ages are available.

Besides the VSL ages for the oldest part of the sequence, several ages were also determined for the youngest samples. Although at first glance, the VSL ages for the subsequent samples Koz5, Koz6, and Koz7 do not seem consistent with the outcome of other dating techniques, their corresponding age intervals overlap one another (at two sigma).

Getting back to the older part of the sequence, we can see an excellent match between IR-RF- and VSL- based results, 279±29 ka and 324±94 ka, respectively for sample Koz14, layer 10c as an example. This picture does not hold for the older ages, however, still within two sigma,

both ages can be considered consistent, given the large error inherent for the VSL ages observed for all samples and related to the shape of the dose-response curve.

The IR-RF ages are more precise (i.e., they show smaller analytical error bars) and are less scattered. The VSL age estimated for the oldest sample Koz21 belonging to layer 13c in the profile was estimated at 704±168 ka. This age seems to be greater than the corresponding age based on IR-RF (387±28 ka), although the large uncertainty obtained for the VSL age, makes a reasonable comparison difficult.

Table 4

Fig. 9.

4. Discussion

4.1 How confident are we about the obtained chronologies?

In the previous section, we presented ages based on different luminescence dating techniques. Since the age discrepancies observed between the various signals were not always negligible, it is worthwhile to critically reflect the ages and discuss reasons for these differences.

The IRSL ages estimated for all three samples led to older ages compared to other results. King et al. (2018) argued that employing a single saturating exponential fit can result in overestimated D_e dependent on the characteristic of the dose-response curve. Nevertheless, it should be noted that a single saturating exponential function perfectly described the dose-response curve for these three samples in this study. A general-order kinetic (GOK, Guralnik et al., 2015) also was tried for fitting sample Koz11 for which the D_e was not located in the linear part of the dose-response curve, and hence varying fitting functions could potentially lead to different outcomes. Applying this fitting resulted in a larger value compared to the single-saturating exponential function.

It is worth mentioning that the GOK can result in more reliable estimation only if the higher part of the dose-response curve is thoroughly defined by incorporating relatively large regenerative points (King et al., 2018). The largest regenerative dose used for generating the dose-response curve for Koz11 was only 600 Gy, while the individual D_e s of ca 600-700 Gy were obtained for this sample. This could justify why applying GOK resulted in a larger D_e, and thus it was not a suitable function for our dataset. Having said that, even if the shape of the dose-response curve is considered problematic for Koz11, for younger samples, Koz4 and Koz8 this is not the case. Therefore, we can argue that it is more likely that the obtained *g*-values are not displaying the true measures and they are possibly overestimated. The proper

estimation of the fading rate in percentage per decade (the *g*-value) is a challenging task and minute variations in temperature and conditions can result in a very different estimate (cf. Kadereit et al. (2020) and the related public discussion). Although the reason behind this is not clear, it is likely that our estimation of the *g*-value, which is based on maximum pausing of only 4 h, was insufficient to properly determine the fading rate in the laboratory.

Previously in section 3.3, it was stated that $pIR_{50}IRSL_{290}$ ages for the upper part of the sequence seemed to be slightly older than the OSL ages. However, the $pIR_{50}IRSL_{290}$ signal may contain a residual dose (hard to bleach signal, Buylaert et al., 2011) contributing to the measured signal and giving rise to overestimated age. Due to the scarce amount of K-feldspar grains, we did not measure residual dose for our samples, however, in the literature, the amount of 5-20 Gy (e.g., Buylaert et al. 2011) was suggested as a reasonable measure. We calculated the residual doses for the upper part of the sequence assuming that the OSL and $pIR_{50}IRSL_{290}$ ages agree with one another. The values ranged from 9 Gy to 29 Gy, consistent with the values suggested by Buylaert et al. (2011). Subtracting this range from the obtained $pIR_{50}IRSL_{290}$ D_e resulted in the ages in excellent accordance with the corresponding quartz OSL ages. Thus, the discrepancies observed earlier between these two series of ages might be related to 'unbleachable' residual doses.

Furthermore, taking into account the slow beaching rate of the $pIR_{50}IRSL_{290}$ signal compared to the OSL signal (Murray et al., 2012), we can safely conclude that the sediment samples were well-bleached before burial. This inference is also supported from the sedimentological perspective since the original nature of the sediments in the cave was identified as loess-derivates and wind-blown loess (Muttoni et al., 2017). Although some scholars have argued that these sediments should be categorised as loess-like and not (primary) loess (Jipa, 2014). In addition, the bleaching rate of IR-RF is also considered similar to $pIR_{50}IRSL_{290}$ (Frouin et al., 2017), hence the IR-RF ages do not suffer from an age overestimation as already observed by an overall concordance between the $pIR_{50}IRSL_{290}$ and IR-RF ages.

The OSL and $pIR_{50}IRSL_{290}$ ages increase gradually along the profile until layer 10a. Afterwards, due to the saturation, no OSL age was reported. Heydari and Guérin, (2018) demonstrated that the Bayesian models implemented in BayLum (Guérin et al., 2021; Philippe et al., 2019) can lead to a more accurate dose estimation when the signal is close or in saturation, compared to 'classical analyses' using the Analyst software. Thus, in the future, it might be worth applying Bayesian modelling on single grain measurements for samples older than layer 10a and comparing the outcomes with other independent ages available based on different signals.

The $pIR_{50}IRSL_{290}$ ages for layer 10b resulted in 161±13 ka (Koz11) and 199±12 ka (Koz12). The corresponding ages for sample Koz11 using IRSL, VSL and IR-RF yielded 250±40 ka, 321±77 ka, 201±17 ka, respectively, all older than $pIR_{50}IRSL_{290}$. Thus, the $pIR_{50}IRSL_{290}$ age for sample Koz11 appears to be underestimated. Albeit the first argument which immediately springs to mind is the possibility of fading, such conjecture was not derived from the rest of the samples, and it does not appear plausible here.

For the next layer (10b), the $pIR_{50}IRSL_{290}$ age (199±12 ka) with a D_e of 416±16 Gy is in excellent accordance with the corresponding age using the IR-RF signal (201±17 ka). The same trend is observed for layer 10c where $pIR_{50}IRSL_{290}$ resulted in 281±19 ka whereas IR-IF exhibited 279±29 ka.

The $pIR_{50}IRSL_{290}$ ages estimated for layer 10c (D_e of 659-671 Gy) were the oldest age obtained using this signal. Afterwards, for the lower layer (11b), measurements clearly show evidence for signal saturation (four aliquots out of six). On the other hand, IR-RF measurement for layer 11b resulted in D_e of 888±23 Gy. Therefore, the interval between 671±36 Gy (the highest D_e estimated based on $pIR_{50}IRSL_{290}$) and 888±23 Gy can be considered as a saturation level for the $pIR_{50}IRSL_{290}$ signal which is consistent with other findings (e.g., Yi et al., 2015). Although in the literature ca. 1,000 Gy was suggested as a threshold for IR-RF (Erfurt and Krbetschek, 2003), comparing this age with the VSL might imply that the signal saturation for IR-RF is around 923±23 Gy (D_e of oldest sample in layer 13c). By looking at the chronological results from layer 11b to the lowermost layer (13c), it is not inconceivable to speculate that we already gradually reached a saturation level IR-RF signal at even above layer (11b) with the D_e of 888±23 Gy. Comparing VSL ages determined for these layers with IR-RFs, could even reinforce this possibility although the large errors presented for VSL ages do not allow for a very precise and decisive conclusion.

More importantly, Muttoni et al. (2017) established a palaeomagnetism sequence for the Kozarnika cave suggesting the layer immediately after 13c lies in the Brunhes-Matuyama boundary with the timing of 780 ka. They also attributed layers 13a-c to layers L6 to L7 in the stratigraphical Danube loess-palaeosol presented in Marković et al. (2015) (their Fig. 16) and the link allows them to speculate that a period of 600-750 ka (early Brunhes) might represent the timeframe for layers 13a-c. Indeed, the silt fraction becomes more and more abundant from layers 11a to 13b, and the Kozarnika area is included in Pontic East European loess (domain V) (see Lehmkuhl et al., 2021). On the other hand, there is no loess near Kozarnika (see Evlogiev, 2007). The closest loess deposit is reported in distances from 60 km to 100 km of

the cave location. Furthermore, silt remobilized in the karst might be considered loess-like (alluvial and aeolian), which extends more in the west than the loess (see for example Jipa, 2014 or the “lössartige und andere Lehme” of Fotakieva & Minkov, 1966). The sediment accumulation of the lower layers of Kozarnika is endocarstic and therefore discontinuous, with gaps posing difficulties to any quantification. Therefore, we cannot invalidate the hypothesis of sedimentary lacks under the magnetic “event" at the lower part of layer 11b (around -6.50 m) as identified by Kovacheva et al. (in Guadelli et al., 2005) and Muttoni et al. (2017). This might place the Brunhes-Matuyama limit at the base of layer 11b and not in layer 13, which is in agreement with the macro-mammals assemblages of layer 11b (Guadelli et al., 2005, in press; Fernandez and Crégut-Bonnoure, 2007; Sirakov et al., 2010).

In either way, this independent chronological data (palaeomagnetism sequence) can be seen as a strong argument supporting the saturation assumption of IR-RF for layer 13. The VSL age of 704±168 ka for layer 13c, agrees with the period of 600-750 ka, however, only due to the very large uncertainty. Apart from that, the agreement of the VSL ages with other independent ages obtained for the Kozarnika sequence tends to confirm the overall accuracy of the VSL ages, which is consistent with the observation of Ankjærgaard et al. (2016).

These large uncertainty margins, resulting from the leverage effect of the signal uncertainty caused by the flat dose-response curve, are the main drawback of the VSL application. However, this might be ameliorated by increasing the number of measured samples to specify a more precise probability density distribution after projecting L_n/T_ns onto the dose-response curve. This may lead to more confidence in the D_e estimates in future studies.

4.2 Unravelling the timing of humans in the cave

The Kozarnika cave contains three main assemblages associated with the Lower, Middle, and Upper Palaeolithic periods. For the Upper Palaeolithic sequence, some radiocarbon dates are available (Guadelli et al., 2005, in press). Although some of these results were provided nearly two decades ago (new procedures have been suggested since then for sample pre-treatments to improve the accuracy and precision of radiocarbon dates e.g., Wood, 2015), comparing these dates as independent ages with luminescence-based ages is still advantageous. The uppermost luminescence-age based on OSL technique resulted in 32±2 ka for layer (5a), and 30±2 ka for the layer below (layer 5b). The available radiocarbon age for layer 5b exhibited 31.2 ka cal. BP (original data from Guadelli et al. (2005) and calibrated from Muttoni et al. (2017)) showing an excellent concordance with OSL ages within uncertainties. New radiocarbon ages

fall in the range of 29,219-30,030 ka cal. BP to 31,919-33,130 ka cal. BP for layer 5a and 36,152-37,276 ka cal. BP to 36,987-39,875 ka cal. BP for layer 5b (Guadelli et al., in press). Following that, layer 5c represents the radiocarbon range of 40-44 ka cal. BP (original data from Guadelli et al., (2005). These results agree with the new radiocarbon ages suggesting a range of 39,998-41,592 ka cal. BP to 42,085-44,541 ka cal. BP (Guadelli et al., in press). Although there is no luminescence age available for this layer, the age of the layer immediately beneath (6/7) yielded 33±2 ka and 35±2 ka. Sequentially the radiocarbon dates for this layer ranged from 42,194-45,025 ka cal. BP to 43,243-54,492 ka cal. BP (Guadelli et al., in press) which is significantly older than the OSL ages.

The OSL ages for the Upper Palaeolithic assemblages (Kozarnikian) uncovered in layer 5a is in good concordance with the radiocarbon age, however the discrepancies between the OSL and radiocarbon ages for layers 5b and 5c (Guadelli et al. in press) are significant. One possible scenario that could explain the discrepancies between the outcome of two distinct dating methods could be the scatter between OSL D_es for each sample (see Fig. 5a as an example). In such a case implementing signal grain measurements which allows for properly applying a broad body of statistical models could be preferable.

Layer 6/7 with OSL ages of 33±2 ka and 35±2 ka and radiocarbon age range of 42-54 ka cal. BP was considered an intermediate level between the Middle and Upper Palaeolithic (Kozarnikian) containing artefacts associated with both affinities. Still, this does not necessarily imply the mixture of Middle and Upper affinities but rather a concatenation of successive and/or alternately rapid occupations (see Guadelli et al., in press for more details). Although such a situation seems infrequent, it has been already observed for example at Mandrin cave (France) or at Buran Kaya III (Crimea) (Silmak et al., 2017).

The layer after 9ab is attributed to the termination of the Middle Palaeolithic period rendering the Mousterian Levallois elements. The OSL age of 43±3 ka established for layer 9ab within uncertainties agrees with the range of 41,030–39,260 ka cal. BP representing the termination of the Mousterian industry after Higham et al. (2014). Heydari et al. (2020) used Bayesian modelling specifically designed for treating OSL samples to reduce age uncertainties attributed to Palaeolithic assemblages. In particular, they combined OSL ages with radiocarbon dates for one Palaeolithic site and obtained chronologies that were more precise (Heydari et al., 2021). Thus, applying Bayesian modelling to treat luminescence ages in combination with radiocarbon dates seems advantageous in this context to improve the precision for the continuous or discontinuous transition timeframe from the Middle to Upper Palaeolithic period.

A remarkable finding in layer 10b was a radius of an infant attributed to a Neanderthal, which earlier was dated between 128 ± 13 ka and 183 ± 14 ka using OSL and $pIR_{50}IRSL_{290}$ techniques (Tillier et al., 2017). Nevertheless, in the present study, we acknowledge that the OSL age of 128 ± 13 ka is underestimated, and we suggest an age of 201±17 ka, based on IR-RF, revealing older deposit of the Neanderthal infant's skeleton. This result confirms the new biochronological interpretation of the middle sequence of Kozarnika cave (Guadelli et al., in press). Nevertheless, a stark contrast for the oldest layers exists between the biochronological framework according to micromammals (Popov and Marinska, 2007) and the one based on large mammal species (Guadelli et al., 2005; Fernandez and Crégut-Bonnoure, 2007; Sirakov et al., 2010).

The Lower Palaeolithic industries were found from layer 11a downwards. The luminescence dating suggested the onset of the Middle Palaeolithic period in the timeframe of 279±29 ka (IR-RF) 324±94 ka (VSL), which is perfectly in line with what we expect from other chronologies established for Middle Palaeolithic assemblages (Richter, 2011).

The youngest ages attributed to the Lower Palaeolithic assemblages in layer 11b were 337±23 ka (IR-RF), and 419±137 ka (VSL) and the oldest ages for layer 13c exhibited 387±28 ka (IR-RF) and 704±168 ka (VSL). Although here luminescence dating is nearly at its age limit, taking into account the smooth increase in the obtained ages along with the profile, does not seem to support a period of 1,400-1,600 ka estimated using large mammal biochronology (Sirakov et al., 2010) for layers 13a-c or even the revisited biochronological estimation of 1,200/1,000-1,400/1,200 ka for the layer 12 to layers 13a-c suggested by Guadelli et al. (in press). Surprisingly, the maximum age of 780 ka also questions the biochronology result for the Lower Palaeolithic sequence of the Kozarnika cave (Brunhes-Matuyama boundary) proposed for layer 13c using palaeomagnetic dating (Muttoni et al., 2017). At this stage, it seems that further chronological work is required to reach a decisive conclusion for the oldest layers of the sequence.

5. Conclusions

A complete chronology for the Kozarnika cave was established using various luminescence-dating techniques. Combining different approaches allowed us to successfully date sediments from ca 30 ka to 700 ka unravelling the timing of human occupations during a large part of the Palaeolithic. Nevertheless, at this stage, we cannot rule out the possibility of underestimated timeframes for the layers containing the Lower Palaeolithic assemblages.

The obtained ages rely on the measurement of different signals for each sample to increase our confidence about the reliability of the outcomes. The overall accordance between the OSL with the $pIR_{50}IRSL_{290}$ ages for the upper part of the sequence makes it likely that both signals were completely bleached before mineral deposition. The same conclusion was deduced for the IR-RF signal, negating the possibility of age overestimation due to the slow beaching rate that often impedes the application of this method.

This study indicates that the saturation dose for the $pIR_{50}IRSL_{290}$ signal (at around 700 Gy to 900 Gy) led to ages of 291±22 ka and 281±19 ka as the oldest ages obtained in Kozarnika using this signal. On the other hand, the IR-RF saturated later, which enabled the age limit to be extended until 387±28 ka for this sequence. Moreover, the IR-RF doses measured on samples from layers 11a to 13c are indistinguishable, which probably indicates signal saturation. In that case, a dose of ~900 Gy might correspond to the field saturation limit of IR-RF for our samples. The IRSL ages were deemed to overestimate other ages presumably due to an inaccurate *g*-value estimate. Applying the VSL technique in combination with MAAD protocol resulted in ages that were consistent with other signal-based ages and implied the trustworthiness of outcomes. The drawback of this application was large uncertainty margins, which could be ameliorated by increasing the number of measured samples, and hence improving the precision. More crucially, Muttoni et al. (2017) assigned the Brunhes–Matuyama reversal (780 ka) to the layer beneath 13c using Palaeomagnetic dating. Subsequently, a timeframe of 600-750 ka was suggested for layers 13a-c (Muttoni et al., 2017) by correlating layers 13a-c to the Danube loess sequence layers L6-L7 (Marković et al., 2015). Thus, the obtained VSL age for layer 13c within error is consistent with that period. However, the large uncertainty on this VSL age renders a precise interpretation difficult. In addition, the independent age available for layers 13a-c (with the range of 600-750 ka) also might indicate that the IR-RF ages represent the minimum age for these layers.

Employing various luminescence signals in this study led to determining the timing of the human inhabitants of Kozarnika cave. The Kozarnikian assemblages discovered in layers 5a-c dates back to 32±2 ka and 33±2 ka. Generally, radiocarbon dates (Guadelli et al., 2005, in press) provided for Kozarnikian assemblages in layers 5a-c and 6/7 are older compared to luminescence dating.

This study revealed that the onset of the Middle Palaeolithic period happened at 279±29 ka (IR-RF) 324±94 ka (VSL) and it lasted until between 49±4 ka and 43±3 ka. The lower Palaeolithic assemblages in Kozarnika cave dated back to between 337±23 ka (IR-RF) and

704±168 ka (VSL). However, due to the supposed limit of luminescence dating in this dose range (setting our upper datable age limit), it is likely that they present minimum ages. Therefore, further chronological investigations using dating methods with extended age limit are required to shed light on the reliability of these ages and to further constrain the timing of the humans who lived during the Lower Palaeolithic period in the Kozarnika cave.

Table 1. Location of the sediment samples taken from the site.

Sample name	Squares	X	Y	Z	Geological layers
Koz1	H7	199.000	1498.900	-4.259	5a
Koz2	H7	199.000	1498.580	-4.570	5b
Koz3	H7	199.000	1498.333	-4.609	5c
Koz4	H6	199.000	1497.632	-4.695	6/7
Koz5	H8	199.000	1499.560	-4.549	6/7
Koz6	H8	199.000	1499.590	-4.744	9ab
Koz7	H7	199.000	1498.580	-4.787	9ab
Koz8	H7	199.000	1498.730	-4.954	9c
Koz9	H8	199.000	1499.560	-4.896	9c
Koz10	H7	199.000	1498.610	-5.078	10a
Koz11	F8	196.000	1499.119	-5.232	10b
Koz12	F7	196.000	1498.325	-5.310	10b
Koz13	H7	199.000	1498.770	-5.259	10c
Koz14	F8	196.000	1499.122	-5.396	10c
Koz16	F8	196.000	1499.107	-5.880	11b
Koz18	G11	197.419	1503.000	-7.437	12
Koz20	G11	197.473	1503.000	-7.551	13a
Koz21	H11	198.000	1502.000	-8.000	13c

Table 2. The concentration of radionuclides obtained through gamma-ray spectrometry.

Sample name	K (%)	U pre-^{226}Ra (ppm)	U post-^{226}Ra (ppm)	Th (ppm)
Koz1	1.58±0.02	1.93±0.08	1.97±0.02	6.83±0.07
Koz2	1.48±0.02	1.17±0.07	1.24±0.02	4.75±0.05
Koz3	1.54±0.02	1.19±0.07	0.99±0.02	4.95±0.06
Koz4	1.47±0.02	1.13±0.07	1.33±0.02	5.26±0.06
Koz5	1.44±0.02	1.11±0.07	1.29±0.02	4.72±0.06
Koz6	2.15±0.02	2.08±0.08	1.64±0.02	7.92±0.07
Koz7	2.06±0.02	1.92±0.07	1.55±0.02	7.63±0.06
Koz8	1.41±0.02	1.14±0.05	1.32±0.01	4.84±0.05
Koz9	1.37±0.02	1.24±0.07	1.13±0.02	4.78±0.05
Koz10	1.35±0.02	1.21±0.07	1.17±0.02	4.95±0.05
Koz11	1.13±0.01	0.88±0.06	0.89±0.01	4.08±0.05
Koz12	1.20±0.01	0.92±0.06	0.91±0.01	4.30±0.05
Koz13	1.29±0.02	1.16±0.07	1.11±0.01	5.64±0.05
Koz14	1.34±0.01	1.25±0.05	1.17±0.01	5.75±0.05

Koz16	1.41±0.01	1.67±0.06	1.39±0.01	6.97±0.06
Koz18	1.60±0.02	1.61±0.07	1.06±0.01	6.47±0.06
Koz20	1.47±0.02	1.75±0.08	1.59±0.02	7.78±0.07
Koz21	1.50±0.02	1.78±0.07	1.76±0.02	8.25±0.07

Table 3. The estimated dose rates for sediment samples in this study.

Sample name	Water content (WF %)	Laboratory Gamma (Gy/ka)	*in situ* Gamma (Gy/ka)	Beta (Gy/ka)	Cosmic (Gy/ka)	Total D_r Quartz (Gy/ka)	Total D_r K-Feldspar (Gy/ka)
Koz1	15±6	0.81±0.03	0.31±0.02	1.31±0.06	0.09±0.01	1.77±0.07	2.61±0.15
Koz2	14±6	0.63±0.02	0.34±0.01	1.13±0.06	0.09±0.01	1.62±0.06	2.45±0.15
Koz3	14±5	0.63±0.02	0.39±0.02	1.17±0.06	0.09±0.01	1.70±0.07	2.54±0.15
Koz4	15±6	0.66±0.02	0.31±0.02	1.14±0.06	0.09±0.01	1.60±0.07	2.44±0.15
Koz5	14±5	0.63±0.02	0.38±0.01	1.12±0.05	0.09±0.01	1.65±0.06	2.48±0.15
Koz6	14±5	0.97±0.03	0.54±0.01	1.70±0.08	0.09±0.01	2.38±0.09	3.22±0.16
Koz7	15±6	0.92±0.03	0.59±0.01	1.61±0.08	0.09±0.01	2.34±0.09	3.18±0.16
Koz8	14±5	0.63±0.02	0.50±0.00	1.11±0.05	0.09±0.01	1.75±0.06	2.59±0.15
Koz9	14±6	0.60±0.02	0.39±0.00	1.06±0.05	0.09±0.01	1.60±0.06	2.44±0.15
Koz10	15±6	0.60±0.02	0.33±0.01	1.05±0.05	0.09±0.01	1.53±0.06	2.36±0.15
Koz11	15±6	0.49±0.02	0.20±0.00	0.86±0.04	0.09±0.01	1.21±0.05	2.05±0.15
Koz12	15±6	0.52±0.02	0.19±0.00	0.92±0.05	0.09±0.01	1.25±0.06	2.09±0.15
Koz13	14±5	0.62±0.02	0.25±0.01	1.03±0.05	0.08±0.01	1.43±0.06	2.26±0.15
Koz14	14±6	0.64±0.02	0.35±0.00	1.06±0.05	0.08±0.01	1.56±0.06	2.39±0.15
Koz16	20±8	0.68±0.03	0.57±0.01	1.09±0.07	0.08±0.01	1.80±0.07	2.64±0.15
Koz18	20±8	0.70±0.03	0.72±0.01	1.19±0.08	0.07±0.01	2.04±0.08	2.87±0.16
Koz20	20±8	0.74±0.03	0.50±0.03	1.16±0.07	0.07±0.01	1.79±0.08	2.62±0.16
Koz21	20±8	0.78±0.04	0.23±0.01	1.20±0.07	0.06±0.01	1.55±0.08	2.39±0.16

Table 4. The D_e and corresponding ages within uncertainties estimated using various luminescence signals.

	OSL		pIR_{50}-$IRSL_{290}$		IRSL		VSL		IR-RF	
Sample names	D_e (Gy)	Age (ka)	D_e (Gy)	Age (ka)	D_e (Gy)	Age (ka)	D_e (Gy)	Age (ka)	D_e (Gy)	Age (ka)
Koz1	57±2	32±2								
Koz2	48±2	30±2	95±3	39±2						
Koz3	56±3	33±2								
Koz4	53±1	33±2	90±3	37±2	109±1	45±3				
Koz5	58±2	35±2								
Koz6	117±9	49±4	176±5	55±3			101±35	42±15		
Koz7	101±6	43±3	162±6	51±3			96±21	41±9		
Koz8	92±4	53±3	158±15	61±6	171±4	66±4	166±119	95±68		
Koz9	82±4	51±3	138±3	57±3						
Koz10	90±5	59±4	168±4	71±4						

Koz11	330±22	161±13	512±72	250±40	390±91	321±77	411±18	201±17
Koz12	416±16	199±12						
Koz13	659±39	291±22						
Koz14	671±36	281±19			504±144	324±94	668±56	279±29
Koz16					755±245	419±137	888±23	337±23
Koz18					768±227	377±113	835±20	290±18
Koz20							906±17	346±23
Koz21					1092±253	704±168	923±23	387±28

Acknowledgements

MH received funding from the GHKO association for her work in early 2016. The work was later supported by the LaScArBx. LaScArBx is a research programme supported by the ANR (ANR-10-LABX-52). Sebastian Kreutzer is thanked for providing the map and his support in analysing the IR-RF measurement data in 2016/2017.

Research in Kozarnika cave was undertaken within the framework of an international cooperation between the National Institute of Archaeology of the Bulgarian Academy of Sciences (N. Sirakov) and the UMR5199 CNRS PACEA (J.-L. Guadelli); the works of this Bulgarian-French cooperation are financially supported by the Advisory Committee of the Archaeological Research abroad of the French Ministry of Foreign Affairs (Mission Paléolithique de Bulgarie - dir. J.-L. Guadelli), by the CNRS (Centre National de la Recherche Scientifique), by the Region Aquitaine, by the University Bordeaux 1 (2004), by the Max Planck Institute for Evolutionary Anthropology, Department of Human Evolution (2004), ERC PALAEOCHRON (Dir. T. Higham) for 14C AMS dates (R. Hopkins, 2015-2018) and by the Bulgarian Academy of Sciences. To all of them, we send our deepest thanks.

Author Contributions

Conceptualization: Maryam Heydari, Guillaume Guérin, Jean-Luc Guadelli
Data curation: Maryam Heydari
Formal analysis: Maryam Heydari
Funding acquisition: Maryam Heydari, Jean-Luc Guadelli
Investigation: Maryam Heydari, Guillaume Guérin, Nikolay Sirakov, Philippe Fernandez, Catherine Ferrier, Aleta Guadelli, Jean-Claude Leblanc, Stanimira Taneva, Svoboda Sirakova, Jean-Luc Guadelli
Methodology: Maryam Heydari, Guillaume Guérin
Project administration: Jean-Luc Guadelli, Guillaume Guérin
Software: Maryam Heydari, Jean-Luc Guadelli
Supervision: Jean-Luc Guadelli, Guillaume Guérin
Visualization: Maryam Heydari, Jean-Luc Guadelli
Roles/Writing - original draft: Maryam Heydari
Writing - review & editing. Maryam Heydari, Jean-Luc Guadelli, Guillaume Guérin, Philippe Fernandez

Figure captions

Fig. 1. The Kozarnika cave is located in the northern hills of the Balkan Mountains, ca 30 km south of the Danube River, in the northwest of Bulgaria.

Fig. 2. Profile picture of the cave where sediment samples were taken from. The obtained luminescence ages according to different techniques are presented here.

Fig. 3. Comparison between the *in situ* and laboratory (gamma-ray spectrometry) gamma dose rate estimates. The *in situ* results are significantly lower compared to the laboratory measurements due to the heterogeneous environment observed in the sediment layers. Since limestone fragments from the bedrock are the source of radiation heterogeneities (limestone is generally poor in radioelements), this systematic discrepancy is expected. Thus, in situ measurements are more representative of the sediment burial conditions.

Fig. 4. Illustrating the dose-response curves for the OSL, $pIR_{50}IRSL_{290}$, and IRSL measurements derived from sample Koz4.

Fig. 5. D_e distributions generated from OSL (A) $pIR_{50}IRSL_{290}$ (B) and $IRSL_{50}$ (C) measurements for sample Koz4 as an example using Abanico plot (Dietze et al., 2016).

Fig. 6. Typical IR-RF curves were obtained for three samples. Each plot represents results for one multiple grain aliquot. The natural signal is indicated by red-filled circles and the regenerated signal by green crosses. The horizontal and vertical sliding was used to estimate the D_e for each subsample.

Fig. 7. The kernel density estimate (KDE) plots for three samples as examples to show typical D_es distributions.

Fig. 8. VSL MAAD dose-response curve. The L/T s for each set of irradiated samples are shown in this figure. For the fitting, we applied a dose-response curve function based on the Lambert W function. The value of 11±12 Gy was obtained using this fitting for sample Koz4 (not irradiated), which within uncertainties is consistent with zero.

Fig. 9. The age-depth plot for all samples in this study covering the period of ca 30 ka to 700 ka using various luminescence signals. To provide better insight into the ages from Koz1 to Koz10 they are depicted in the inset.

References

Alex, B., Mihailović, D., Milošević, S., Boaretto, E., 2019. Radiocarbon chronology of Middle and Upper Paleolithic sites in Serbia, Central Balkans. Journal of Archaeological Science: Reports 25, 266–279. https://doi.org/10.1016/j.jasrep.2019.04.010

Ankjærgaard, C., Guralnik, B., Buylaert, J.-P., Reimann, T., Yi, S.W., Wallinga, J., 2016. Violet stimulated luminescence dating of quartz from Luochuan (Chinese loess plateau): Agreement with independent chronology up to ∼600 ka. Quaternary Geochronology 34, 33–46. https://doi.org/10.1016/j.quageo.2016.03.001

Ankjærgaard, C., Jain, M., Wallinga, J., 2013. Towards dating Quaternary sediments using the quartz Violet Stimulated Luminescence (VSL) signal. Quaternary Geochronology 18, 99–109. https://doi.org/10.1016/j.quageo.2013.06.001

Bortolot, V.J., 2000. A new modular high capacity OSL reader system. Radiation Measurements 32, 751–757. https://doi.org/10.1016/S1350-4487(00)00038-X

Bos, A.J.J., Wallinga, J., 2012. How to visualize quartz OSL signal components. Radiation Measurements 47, 752–758. https://doi.org/10.1016/j.radmeas.2012.01.013

Bøtter-Jensen, L., Andersen, C.E., Duller, G.A.T., Murray, A.S., 2003. Developments in radiation, stimulation and observation facilities in luminescence measurements. Radiation Measurements 37, 535–541. https://doi.org/10.1016/S1350-4487(03)00020-9

Bulur, E., 1996. An alternative technique for optically stimulated luminescence (OSL) experiment. Radiation Measurements 26, 701–709. https://doi.org/10.1016/s1350-4487(97)82884-3

Buylaert, J.-P., Jain, M., Murray, A.S., Thomsen, K.J., Thiel, C., Sohbati, R., 2012. A robust feldspar luminescence dating method for Middle and Late Pleistocene sediments: Feldspar luminescence dating of Middle and Late Pleistocene sediments. Boreas 41, 435–451. https://doi.org/10.1111/j.1502-3885.2012.00248.x

Buylaert, J.P., Thiel, C., Murray, A.S., Vandenberghe, D.A.G., Yi, S., Lu, H., 2011. IRSL and post-IR IRSL residual doses recorded in modern dust samples from the Chinese Loess Plateau. Geochronometria 38, 432–440. https://doi.org/10.2478/s13386-011-0047-0

Devièse, T., Karavanić, I., Comeskey, D., Kubiak, C., Korlević, P., Hajdinjak, M., Radović, S., Procopio, N., Buckley, M., Pääbo, S., Higham, T., 2017. Direct dating of Neanderthal remains from the site of Vindija Cave and implications for the Middle to Upper Paleolithic transition. Proc Natl Acad Sci USA 114, 10606–10611. https://doi.org/10.1073/pnas.1709235114

Dietze, M., Kreutzer, S., Burow, C., Fuchs, M.C., Fischer, M., Schmidt, C., 2016. The abanico plot: Visualising chronometric data with individual standard errors. Quaternary Geochronology 31, 12–18. https://doi.org/10.1016/j.quageo.2015.09.003

Doronichev, V.B., 2008. The Lower Paleolithic in Eastern Europe and the Caucasus: A Reappraisal of the Data and New Approaches. PaleoAnthropology, 107–157.

Duller, G.A.T., 2015. The Analyst software package for luminescence data: overview and recent improvements. Ancient TL 33, 35-42.

Duller, G.A.T., 2003. Distinguishing quartz and feldspar in single grain luminescence measurements. Radiation Measurements 37, 161–165. https://doi.org/10.1016/S1350-4487(02)00170-1

Erfurt, G., Krbetschek, M.R., 2003. IRSAR – A single-aliquot regenerative-dose dating protocol applied to the infrared radiofluorescence (IR-RF) of coarse- grain K-feldspar. Ancient TL 21, 35-42.

Evlogiev, Y. 2007. Evidence for the Aeolian origin of loess in the Danubian Plain. *Geologica Balcanica* 36 (3-4), 31-39.

Fernandez, P., Crégut-Bonnoure, E., 2007. Les Caprinae (Rupicaprini, Ovibovini, Ovini et Caprini) de la séquence pléistocène de Kozarnika (Bulgarie du Nord): morphométrie, biochronologie et implications phylogéniques. *Revue de Paléobiologie* 26, 2, 425-503. http://halshs.archives-ouvertes.fr/halshs-00284574/en/

Ferrier, Leblanc, J.-Cl, Berthet, A.-L, Delfour, G, 2009. Kozarnika. Etude geologique et sedimentologique. Avalon, Sofia, pp. 13-27, In: Gatsov, I., Guadelli, J.-L. (Eds.), Saxa Loquuntur! "The stone will speak!".

Fewlass, H., Talamo, S., Wacker, L., Kromer, B., Tuna, T., Fagault, Y., Bard, E., McPherron, S.P., Aldeias, V., Maria, R., Martisius, N.L., Paskulin, L., Rezek, Z., Sinet-Mathiot, V., Sirakova, S., Smith, G.M., Spasov, R., Welker, F., Sirakov, N., Tsanova, T., Hublin, J.-J., 2020. A 14C chronology for the Middle to Upper Palaeolithic transition at Bacho Kiro Cave, Bulgaria. Nat Ecol Evol 4, 794–801. https://doi.org/10.1038/s41559-020-1136-3

Fotakieva, E.M., Minkov, M. 1966. Der Löß in Bulgarien. Eiszeitalter und Gegenwart. Band 17, 87-96, 3 abb., 1 tab.

Frouin, M., Huot, S., Kreutzer, S., Lahaye, C., Lamothe, M., Philippe, A., Mercier, N., 2017. An improved radiofluorescence single-aliquot regenerative dose protocol for K-feldspars. Quaternary Geochronology 38, 13–24. https://doi.org/10.1016/j.quageo.2016.11.004

Fu, Q., Hajdinjak, M., Moldovan, O.T., Constantin, S., Mallick, S., Skoglund, P., Patterson, N., Rohland, N., Lazaridis, I., Nickel, B., Viola, B., Prüfer, K., Meyer, M., Kelso, J., Reich, D., Pääbo, S., 2015. An early modern human from Romania with a recent Neanderthal ancestor. Nature 524, 216–219. https://doi.org/10.1038/nature14558

Galanidou, N., 2004. Early Hominids in the Balkans, in: Griffiths, H.I., Kryštufek, B., Reed, J.M. (Eds.), Balkan Biodiversity. Springer Netherlands, Dordrecht, pp. 147–165. https://doi.org/10.1007/978-1-4020-2854-0_9

Glen, E., Kaczanowski, K., 1982. Human remains. In: Excavation in the Bacho Kiro Cave (Bulgaria). Final Report. J. Kozlowski (ed.). Panstwowe Wydawnictwo Naukowe, Warszawa 75–79.

Guadelli, J.L., Sirakov, N., Ivanova, S., Sirakova, S., Anastassova, E., Courtaud, P., Dimitrova, I., Djabarska, N., Fernandez, P., Ferrier, C., Fontugne, M., Gambier, D., Guadelli, A., Iordanova, D., Iordanova, N., Kovatcheva, M., Krumov, I., Leblanc, J.C., Mallye, J.B., Marinska, M., Miteva, V., Popov, V., Spasov, R., Taneva, S., Tisterat-Laborde, N., Tsanova, T., 2005. Une séquence du Paléolithique inferieur au Paléolithique récent dans les balkans : La grotte kozarnika à oreshets (nord-ouest de la bulgarie), in: Molines, N, Moncel, M.H., undefined, Monnier, J.L. (Eds.), Les Premiers Peuplements En Europe. BAR, pp. 87–103.

Guadelli, J.-L., Sirakov, N., Delpech F., Dimitrova, I., Fernandez, P., Ferrier, C., Guadelli, A., Krumov, I., Leblanc, J.-Cl., Sirakova, S., Taneva, S., Tillier A.-m. In press. Earliest dispersals and migrations to Europe via the Balkans in Lower to Upper Palaeolithic: Evidence from Kozarnika Cave (Northern Bulgaria). *Symposium : Évolution de la biodiversité depuis plus d'un million d'années et rapports entre l'Homme et son environnement sur le littoral méditerranéen*. Nice 01-02 octobre 2020. 64p., 28 fig., 20 tab.

Guérin, G., Christophe, C., Philippe, A., Murray, A.S., Thomsen, K.J., Tribolo, C., Urbanova, P., Jain, M., Guibert, P., Mercier, N., Kreutzer, S., Lahaye, C., 2017. Absorbed dose, equivalent dose, measured dose rates, and implications for OSL age estimates: Introducing the Average Dose Model. Quaternary Geochronology 41, 163–173. https://doi.org/10.1016/j.quageo.2017.04.002

Guérin, G., Lahaye, C., Heydari, M., Autzen, M., Buylaert, J.-P., Guibert, P., Jain, M., Kreutzer, S., Lebrun, B., Murray, A.S., Thomsen, K.J., Urbanova, P., Philippe, A., 2021. Towards an improvement of optically stimulated luminescence (OSL) age uncertainties: modelling OSL ages with systematic errors, stratigraphic constraints and radiocarbon ages using the R package BayLum. Geochronology 3, 229–245. https://doi.org/10.5194/gchron-3-229-2021

Guérin, G., Mercier, N., 2012. Preliminary insight into dose deposition processes in sedimentary media on a scale of single grains: Monte Carlo modelling of the effect of water on the gamma dose rate. Radiation Measurements 47, 541–547. https://doi.org/10.1016/j.radmeas.2012.05.004

Guérin, G., Mercier, N., Adamiec, G., 2011. Dose-rate conversion factors: update. Ancient TL 29, 5–8.

Guérin, G., Mercier, N., Nathan, R., Adamiec, G., Lefrais, Y., 2012. On the use of the infinite matrix assumption and associated concepts: A critical review. Radiation Measurements 47, 778–785. https://doi.org/10.1016/j.radmeas.2012.04.004

Guibert, P., Lahaye, C., Bechtel, F., 2009. The importance of U-series disequilibrium of sediments in luminescence dating: A case study at the Roc de Marsal Cave (Dordogne, France). Radiation Measurements 44, 223–231. https://doi.org/10.1016/j.radmeas.2009.03.024

Guibert, P., Schvoerer, M., 1991. TL dating: Low background gamma spectrometry as a tool for the determination of the annual dose. International Journal of Radiation Applications and Instrumentation. Part D. Nuclear Tracks and Radiation Measurements 18, 231–238. https://doi.org/10.1016/1359-0189(91)90117-Z

Guralnik, B., Jain, M., Herman, F., Ankjærgaard, C., Murray, A.S., Valla, P.G., Preusser, F., King, G.E., Chen, R., Lowick, S.E., Kook, M., Rhodes, E.J., 2015. OSL-thermochronometry of feldspar from the KTB borehole, Germany. Earth and Planetary Science Letters 423, 232–243. https://doi.org/10.1016/j.epsl.2015.04.032

Hajdinjak, M., Mafessoni, F., Skov, L., Vernot, B., Hübner, A., Fu, Q., Essel, E., Nagel, S., Nickel, B., Richter, J., Moldovan, O.T., Constantin, S., Endarova, E., Zahariev, N., Spasov, R., Welker, F., Smith, G.M., Sinet-Mathiot, V., Paskulin, L., Fewlass, H., Talamo, S., Rezek, Z., Sirakova, S., Sirakov, N., McPherron, S.P., Tsanova, T., Hublin, J.-J., Peter, B.M., Meyer, M., Skoglund, P., Kelso, J., Pääbo, S., 2021. Initial Upper Palaeolithic humans in Europe had recent Neanderthal ancestry. Nature 592, 253–257. https://doi.org/10.1038/s41586-021-03335-3

Hansen, V., Murray, A., Buylaert, J.-P., Yeo, E.-Y., Thomsen, K., 2015. A new irradiated quartz for beta source calibration. Radiation Measurements 81, 123–127. https://doi.org/10.1016/j.radmeas.2015.02.017

Heydari, M., Guérin, G., 2018. OSL signal saturation and dose rate variability: Investigating the behaviour of different statistical models. Radiation Measurements 120, 96–103. https://doi.org/10.1016/j.radmeas.2018.05.005

Heydari, M., Guérin, G., Kreutzer, S., Jamet, G., Kharazian, M.A., Hashemi, M., Nasab, H.V., Berillon, G., 2020. Do Bayesian methods lead to more precise chronologies? 'BayLum' and a first OSL-based chronology for the Palaeolithic open-air site of Mirak (Iran). Quaternary Geochronology 59, 101082. https://doi.org/10.1016/j.quageo.2020.101082

Heydari, M., Guérin, G., Zeidi, M., Conard, N.J., 2021. Bayesian luminescence dating at Ghār-e Boof, Iran, provides a new chronology for Middle and Upper Paleolithic in the southern Zagros. Journal of Human Evolution 151, 102926. https://doi.org/10.1016/j.jhevol.2020.102926

Higham, T., Douka, K., Wood, R., Ramsey, C.B., Brock, F., Basell, L., Camps, M., Arrizabalaga, A., Baena, J., Barroso-Ruíz, C., Bergman, C., Boitard, C., Boscato, P.,

Caparrós, M., Conard, N.J., Draily, C., Froment, A., Galván, B., Gambassini, P., Garcia-Moreno, A., Grimaldi, S., Haesaerts, P., Holt, B., Iriarte-Chiapusso, M.-J., Jelinek, A., Jordá Pardo, J.F., Maíllo-Fernández, J.-M., Marom, A., Maroto, J., Menéndez, M., Metz, L., Morin, E., Moroni, A., Negrino, F., Panagopoulou, E., Peresani, M., Pirson, S., de la Rasilla, M., Riel-Salvatore, J., Ronchitelli, A., Santamaria, D., Semal, P., Slimak, L., Soler, J., Soler, N., Villaluenga, A., Pinhasi, R., Jacobi, R., 2014. The timing and spatiotemporal patterning of Neanderthal disappearance. Nature 512, 306–309. https://doi.org/10.1038/nature13621

Higham, T., Ramsey, C.B., Karavanic, I., Smith, F.H., Trinkaus, E., 2006. Revised direct radiocarbon dating of the Vindija G1 Upper Paleolithic Neandertals. PNAS 103(3), 553-557.

Hoffecker, J.F., 2009. The spread of modern humans in Europe. Proceedings of the National Academy of Sciences 106, 16040–16045. https://doi.org/10.1073/pnas.0903446106

Hublin, J.-J., Sirakov, N., Aldeias, V., Bailey, S., Bard, E., Delvigne, V., Endarova, E., Fagault, Y., Fewlass, H., Hajdinjak, M., Kromer, B., Krumov, I., Marreiros, J., Martisius, N.L., Paskulin, L., Sinet-Mathiot, V., Meyer, M., Pääbo, S., Popov, V., Rezek, Z., Sirakova, S., Skinner, M.M., Smith, G.M., Spasov, R., Talamo, S., Tuna, T., Wacker, L., Welker, F., Wilcke, A., Zahariev, N., McPherron, S.P., Tsanova, T., 2020. Initial Upper Palaeolithic Homo sapiens from Bacho Kiro Cave, Bulgaria. Nature 581, 299–302. https://doi.org/10.1038/s41586-020-2259-z

Huntley, D.I., Baril, M., 1997. The K content of the K-feldspars being measured in optical dating or in thermoluminescence dating. Ancient TL 15, 11–13.

Huntley, D.J., 2006. An explanation of the power-law decay of luminescence. J. Phys.: Condens. Matter 18, 1359–1365. https://doi.org/10.1088/0953-8984/18/4/020

Huntley, D.J., Godfrey-Smith, D.I., Thewalt, M.L.W., 1985. Optical dating of sediments. Nature 313, 105–107. https://doi.org/10.1038/313105a0

Huntley, D.J., Lamothe, M., 2001. Ubiquity of anomalous fading in K-feldspars and the measurement and correction for it in optical dating. Canadian Journal of Earth Sciences 38, 1093–1106

Hütt, G., Jaek, I., Tchonka, J., 1988. Optical dating: K-feldspars optical response stimulation spectra. Quaternary Science Reviews 7, 381–385. https://doi.org/10.1016/0277-3791(88)90033-9

Jain, M., 2009. Extending the dose range: Probing deep traps in quartz with 3.06eV photons. Radiation Measurements 44, 445–452. https://doi.org/10.1016/j.radmeas.2009.03.011

Jain, M., Murray, A.S., Bøtter-Jensen, L., 2003. Characterisation of blue-light stimulated luminescence components in different quartz samples: implications for dose measurement. Radiation Measurements 37, 441–449. https://doi.org/10.1016/S1350-4487(03)00052-0

Jipa, D.C., 2014. The loess-like deposits in the Lower Danube basin. Genetic signif- icance. Geo-Eco-Marina 20, 7–18.

Kadereit, A., Kreutzer, S., Schmidt, C., DeWitt, R., 2020. A closer look at IRSL SAR fading data and their implication for luminescence dating. Geochronology Discussions 2020, 1–30. https://doi.org/10.5194/gchron-2020-3

Kars, R.H., Wallinga, J., Cohen, K.M., 2008. A new approach towards anomalous fading correction for feldspar IRSL dating — tests on samples in field saturation. Radiation Measurements 43, 786–790. https://doi.org/10.1016/j.radmeas.2008.01.021

King, G.E., Burow, C., Roberts, H.M., Pearce, N.J.G., 2018. Age determination using feldspar: Evaluating fading-correction model performance. Radiation Measurements 119, 58–73. https://doi.org/10.1016/j.radmeas.2018.07.013

Kreutzer, S., Burow, C., Dietze, M., Fuchs, M.C., Schmidt, C., Fischer, M., Friedrich, J., Mercier, N., Smedley, R.K., Christophe, C., Zink, A., Durcan, J., King, G.E., Philippe, A., Guérin, G., Riedesel, S., Autzen, M., Guibert, P., Mittelstrass, D., Gray, H.J., 2021. Luminescence: Comprehensive Luminescence Dating Data Analysis. Zenodo. https://doi.org/10.5281/zenodo.4729933

Kreutzer, S., Martin, L., Guérin, G., Tribolo, C., Selva, P., Mercier, N., 2018. Environmental dose rate determination using a passive dosimeter: Techniques and workflow for α-Al2O3:C chips. Geochronometria 45, 56–67. https://doi.org/10.1515/geochr-2015-0086

Kreutzer, S., Murari, M., Frouin, M., Fuchs, M., Mercier, N., 2017. Always remain suspicious: a case study on tracking down a technical artefact while measuring IR-RF. Ancient TL 35, 20–30.

Kreutzer, S., Schmidt, C., Fuchs, Margret, Dietze, M., Fischer, M., Fuchs, Markus, 2012. Introducing an R package for luminescence dating analysis Ancient TL 30, 1–8

Lehmkuhl, F., Nett, J.J., Pötter, S., Schulte, P., Sprafke, T., Jary, Z., Antoine, P., Wacha, L., Wolf, D., Zerboni, A., Hosek, J.,Markovic, S.B., Obreht, I., Sümegi, P., Veres, D., Zeeden, C., Boemke, B., Schaubert, V., Viehweger, J., Hambach, U. 2021. Loess landscapes of Europe – Mapping, geomorphology, and zonal differentiation. *Earth-Science Reviews*. 215 (2021), 42p., 21 fig., 1 tab. http://dx.doi.org/10.1016/j.earscirev.2020.103496

Li, B., Li, S.-H., 2011. Luminescence dating of K-feldspar from sediments: A protocol without anomalous fading correction. Quaternary Geochronology 6, 468–479. https://doi.org/10.1016/j.quageo.2011.05.001

Marković, S.B., Stevens, T., Kukla, G.J., Hambach, U., Fitzsimmons, K.E., Gibbard, P., Buggle, B., Zech, M., Guo, Z., Hao, Q., Wu, H., O'Hara Dhand, K., Smalley, I.J., Újvári, G., Sümegi, P., Timar-Gabor, A., Veres, D., Sirocko, F., Vasiljević, D.A., Jary, Z., Svensson, A., Jović, V., Lehmkuhl, F., Kovács, J., Svirčev, Z., 2015. Danube loess stratigraphy — Towards a pan-European loess stratigraphic model. Earth-Science Reviews 148, 228–258. https://doi.org/10.1016/j.earscirev.2015.06.005

Mejdahl, V, 1987. Internal radioactivity in quartz and feldspar grains. Ancient TL 5, 10–17.

Murari, M.K., Kreutzer, S., Fuchs, M., 2018. Further investigations on IR-RF: Dose recovery and correction. Radiation Measurements 120, 110–119. https://doi.org/10.1016/j.radmeas.2018.04.017

Murari, M.K., Kreutzer, S., King, G., Frouin, M., Tsukamoto, S., Schmidt, C., Lauer, T., Klasen, N., Richter, D., Friedrich, J., Mercier, N., Fuchs, M., 2021. Infrared radiofluorescence (IR-RF) dating: A review. Quaternary Geochronology 64, 101155. https://doi.org/10.1016/j.quageo.2021.101155

Murray, A.S., Thomsen, K.J., Masuda, N., Buylaert, J.P., Jain, M., 2012. Identifying well-bleached quartz using the different bleaching rates of quartz and feldspar luminescence signals. Radiation Measurements 47, 688–695. https://doi.org/10.1016/j.radmeas.2012.05.006

Murray, A.S., Wintle, A.G., 2000. Luminescence dating of quartz using an improved single-aliquot regenerative-dose protocol. Radiation Measurements 32, 57–73. https://doi.org/10.1016/S1350-4487(99)00253-X

Muttoni, G., Sirakov, N., Guadelli, J.-L., Kent, D.V., Scardia, G., Monesi, E., Zerboni, A., Ferrara, E., 2017. An early Brunhes (<0.78 Ma) age for the Lower Paleolithic tool-bearing Kozarnika cave sediments, Bulgaria. Quaternary Science Reviews 178, 1–13.

Nathan, R.P., Mauz, B., 2008. On the dose-rate estimate of carbonate-rich sediments for trapped charge dating. Radiation Measurements 43, 14–25. https://doi.org/10.1016/j.radmeas.2007.12.012

Nelson, M.S., Rittenour, T.M., 2015. Using grain-size characteristics to model soil water content: Application to dose-rate calculation for luminescence dating. Radiation Measurements 81, 142–149. https://doi.org/10.1016/j.radmeas.2015.02.016

Pagonis, V., Kitis, G., Chen, R., 2020. A new analytical equation for the dose response of dosimetric materials, based on the Lambert W function. Journal of Luminescence 225, 117333. https://doi.org/10.1016/j.jlumin.2020.117333

Philippe, A., Guérin, G., Kreutzer, S., 2019. BayLum - An R package for Bayesian analysis of OSL ages: An introduction. Quaternary Geochronology 49, 16–24. https://doi.org/10.1016/j.quageo.2018.05.009

Popov, V.V., Marinska, M., 2007. An almost one million year long (Early to Late Pleistocene) small mammal succession from the archaeological layers of Kozarnika Cave in Northern Bulgaria. Courier Forschungsinstitut Senckenberg 259, 1, 79–92.

Popov (Попов), 1933. The Mirizlivka cave. Contribution to the diluvial fauna and the culture of the diluvial man in Bulgaria.Попов, Р., 1933. Пещерата Миризливка. Приносъ къмъ дилувиалната фауна и културата на дилувиалния човекъ въ България. National Archaeological Museum (Sofia, Bulgaria) Издания на народния археологически музей. 26, 5–69.

Prescott, J.R., Hutton, J.T., 1994. Cosmic ray contributions to dose rates for luminescence and ESR dating: Large depths and long-term time variations. Radiation Measurements 23, 497–500. https://doi.org/10.1016/1350-4487(94)90086-8

Prescott, J.R., Stephan, L.G., 1982. The contribution of cosmic radiation to the environmental dose for thermoluminescence dating. Latitude, altitude and depth dependences. Journal of the European Study Group on Physical, Chemical and Mathematical Techniques Applied to Archaeology (PACT) 6, 17–25.

Preusser, F., Degering, D., Fuchs, M., Hilgers, A., Kadereit, A., Klasen, N., Krbetschek, M., Richter, D., Spencer, J.Q.G., 2008. Luminescence dating: basics, methods and applications. E&G Quaternary Sci. J. 57, 95–149. https://doi.org/10.3285/eg.57.1-2.5

R Core Team, 2021. R: A language and environment for statistical computing.

Richter, D., Richter, A., Dornich, K., 2015. Lexsyg smart — a luminescence detection system for dosimetry, material research and dating application. Geochronometria 42, 202–209. https://doi.org/10.1515/geochr-2015-0022

Richter, D., Richter, A., Dornich, K., 2013. lexsyg — a new system for luminescence research. Geochronometria 40, 220–228. https://doi.org/10.2478/s13386-013-0110-0

Richter, J., 2011. When Did the Middle Paleolithic Begin?, in: Conard, N.J., Richter, J. (Eds.), Neanderthal Lifeways, Subsistence and Technology, Vertebrate Paleobiology and Paleoanthropology. Springer Netherlands, Dordrecht, pp. 7–14. https://doi.org/10.1007/978-94-007-0415-2_2

Sirakov, N., Tsanova, T., Sirakova, S., Taneva, S., Krumov, I., Dimitrova I., Kovatcheva, N., 2007. Un nouveau faciès lamellaire du début du Paléolithique supérieur dans les Balkans. Paleo 19, 131–144. https://doi.org/10.4000/paleo.565

Sirakov, N., Guadelli, J.-L., Ivanova, S., Sirakova, S., Boudadi-Maligne, M., Dimitrova, I., Ph, F., Ferrier, C., Guadelli, A., Iordanova, D., Iordanova, N., Kovatcheva, M., Krumov, I., Leblanc, J.-Cl., Miteva, V., Popov, V., Spassov, R., Taneva, S., Tsanova, T., 2010. An ancient continuous human presence in the Balkans and the beginnings of human settlement in western Eurasia: A Lower Pleistocene example of the Lower Palaeolithic levels in Kozarnika cave (North-western Bulgaria). Quaternary International 223–224, 94–106. https://doi.org/10.1016/j.quaint.2010.02.023

Slimak, L., Metz , L., Teyssandier, N., 2017. De la fin du Paléolithique moyen aux prémices du Paléolithique supérieur, pénombres et éclairages européens. Le troisième Homme.

Préhistoire de l'Altaï. J.J. Cleyet−Merle, M.V. Shunkov, J.M. Geneste, A.P. Derevianko, L. Slimak, A.L. Krivoshapkin, B. Gravina, A. Turq, B. Maureille eds. Éditions de la Réunion des musées nationaux – Grand Palais, pp. 125–133, 5 fig.

Strait, D.S., Orr, C.M., Hodgkins, J., Spassov, N., Gurova, M., Miller, C., Tzankov, T., 2016. The Human Fossil Record of Bulgaria and the Formulation of Biogeographic Hypotheses, in: Harvati, K., Roksandic, M. (Eds.), Paleoanthropology of the Balkans and Anatolia, Vertebrate Paleobiology and Paleoanthropology. Springer Netherlands, Dordrecht, pp. 69–78. https://doi.org/10.1007/978-94-024-0874-4_5

Thiel, C., Buylaert, J.-P., Murray, A., Terhorst, B., Hofer, I., Tsukamoto, S., Frechen, M., 2011. Luminescence dating of the Stratzing loess profile (Austria) – Testing the potential of an elevated temperature post-IR IRSL protocol. Quaternary International 234, 23–31. https://doi.org/10.1016/j.quaint.2010.05.018

Thomsen, K., Murray, A., Jain, M., 2011. Stability of IRSL signals from sedimentary K-feldspar samples. Geochronometria 38, 1–13. https://doi.org/10.2478/s13386-011-0003-z

Thomsen, K.J., Murray, A.S., Jain, M., Bøtter-Jensen, L., 2008. Laboratory fading rates of various luminescence signals from feldspar-rich sediment extracts. Radiation Measurements 43, 1474–1486. https://doi.org/10.1016/j.radmeas.2008.06.002

Tillier, A., Sirakov, N., Guadelli, A., Fernandez, P., Sirakova, S., Dimitrova, I., Ferrier, C., Guérin, G., Heidari, M., Krumov, I., Leblanc, J.-C., Miteva, V., Popov, V., Taneva, S., Guadelli, J.-L., 2017. Evidence of Neanderthals in the Balkans: The infant radius from Kozarnika Cave (Bulgaria). Journal of Human Evolution 111, 54–62. https://doi.org/10.1016/j.jhevol.2017.06.002

Trautmann, T., Dietrich, A., Stolz, W., Krbetschek, M.R., 1999a. Radioluminescence Dating: A New Tool for Quaternary Geology and Archaeology. Naturwissenschaften 86, 441–444. https://doi.org/10.1007/s001140050649

Trautmann, T., Krbetschek, M.R., Dietrich, A., Stolz, W., 1999b. Feldspar radioluminescence: a new dating method and its physical background. Journal of Luminescence 85, 45–58. https://doi.org/10.1016/S0022-2313(99)00152-0

Trautmann, T., Krbetschek, M.R., Dietrich, A., Stolz, W., 1998. Investigations of feldspar radioluminescence: potential for a new dating technique. Radiation Measurements 29, 421–425. https://doi.org/10.1016/S1350-4487(98)00012-2

Trinkaus, E., Moldovan, O., Milota, S., Bilgar, A., Sarcina, L., Athreya, S., Bailey, S.E., Rodrigo, R., Mircea, G., Higham, T., Ramsey, C.B., van der Plicht, J., 2003. An early modern human from the Pestera cu Oase, Romania. Proceedings of the National Academy of Sciences 100, 11231–11236. https://doi.org/10.1073/pnas.2035108100

Tsanova, T. 2006. Les débuts du Paléolithique supérieur dans l'Est des Balkans. Réflexion à partir de l'étude taphonomique et techno-économique des ensembles lithiques des sites de Bacho Kiro (couche 11), Temnata (couches VI et 4) et Kozarnika (niveau VII). Thèse de doctorat de l' Université Bordeaux 1, 543 pages.

Wintle, A.G., 1973. Anomalous fading of thermoluminescence in mineral samples. Nature 245, 143–144. https://doi.org/10.1038/245143a0

Wood, R., 2015. From revolution to convention: the past, present and future of radiocarbon dating. Journal of Archaeological Science 56, 61–72. https://doi.org/10.1016/j.jas.2015.02.019

Yi, S., Buylaert, J.-P., Murray, A.S., Thiel, C., Zeng, L., Lu, H., 2015. High resolution OSL and post-IR IRSL dating of the last interglacial–glacial cycle at the Sanbahuo loess site (northeastern China). Quaternary Geochronology 30, 200–206. https://doi.org/10.1016/j.quageo.2015.02.013

Figure

Click here to access/download;Figure;Figure1.png

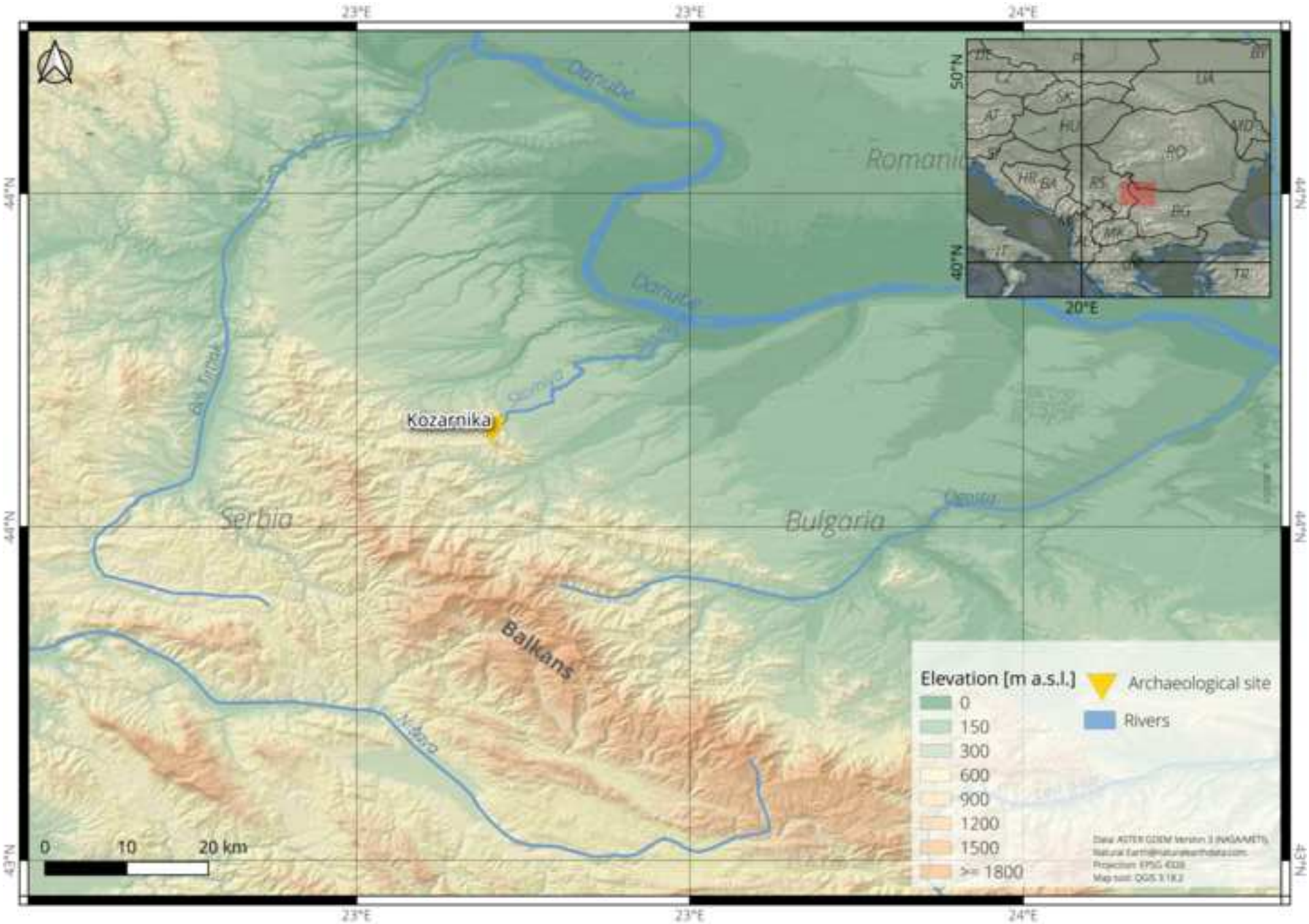

Figure

Click here to access/download;Figure;Figure2.pdf

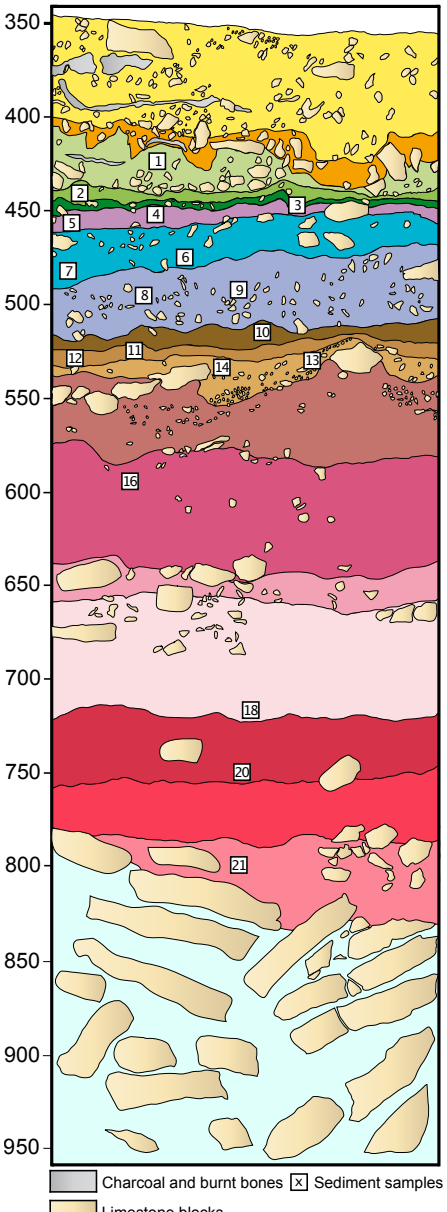

		OSL	IR-RF	VSL	pIRIR
	Koz 1	32±2 ka			
	Koz 2	30±2 ka			
3a 3b	Koz 3	33±2 ka			
	Koz 4	33±2 ka			
4 5a	Koz 5	35±2 ka			
5b 5c	Koz 6	49±4 ka			
6/7 9ab	Koz 7	43±3 ka			
	Koz 8	53±3 ka			
9c	Koz 9	51±3 ka			
10a 10b 10c	Koz 10	59±4 ka			
	Koz 11		201±17 ka	321±77 ka	161±13 ka
11a	Koz 12				199±12 ka
	Koz 13				291±22 ka
	Koz 14		279±29 ka	324±94 ka	281±19 ka
11b	Koz 16		337±23 ka	419±137 ka	
11c					
12					
	Koz 18		290±18 ka	377±113 ka	
13a					
	Koz 20		346±23 ka		
13b					
	Koz 21		387±28 ka	704±168 ka	
13c					
14, 15 & 16					

Figure

Click here to access/download;Figure;Figure3.

Click here to access/download;Figure;Figure4.pdf

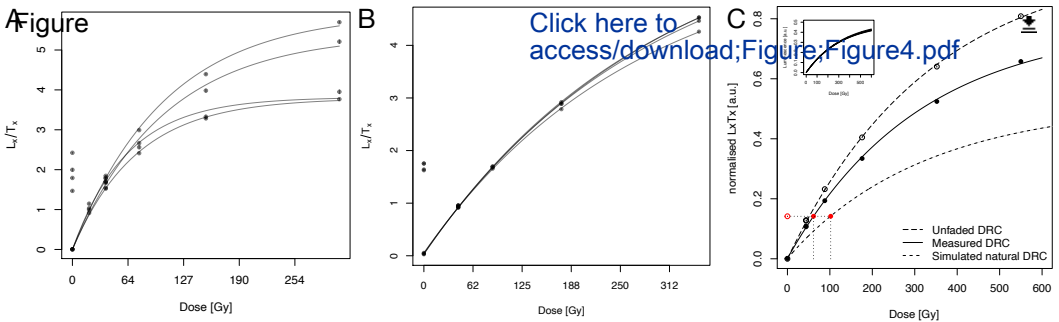

Click here to access/download;Figure;Figure5.pdf

Figure

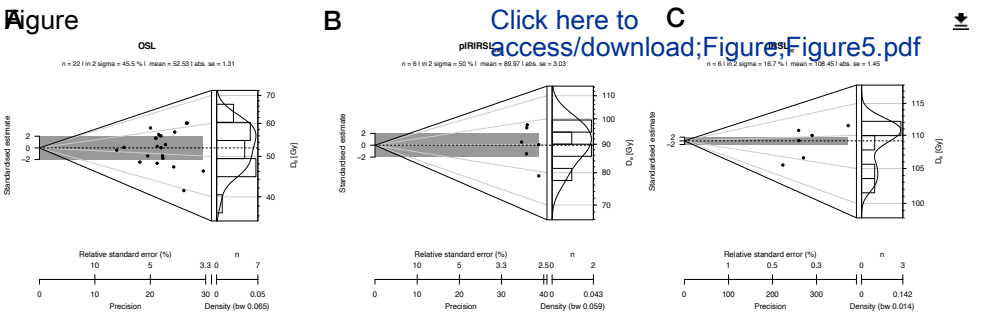

Click here to access/download;Figure;Figure6.pdf

Figure

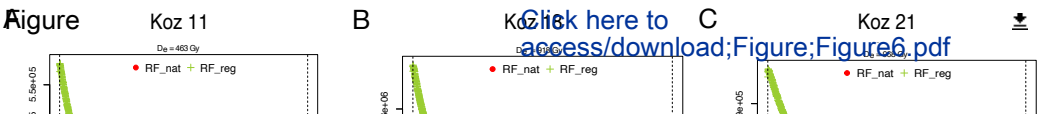

Figure

Click here to access/download;Figure;Figure7.pdf

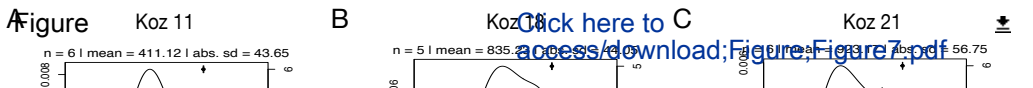

Figure

Click here to access/download;Figure;Figure8.pdf

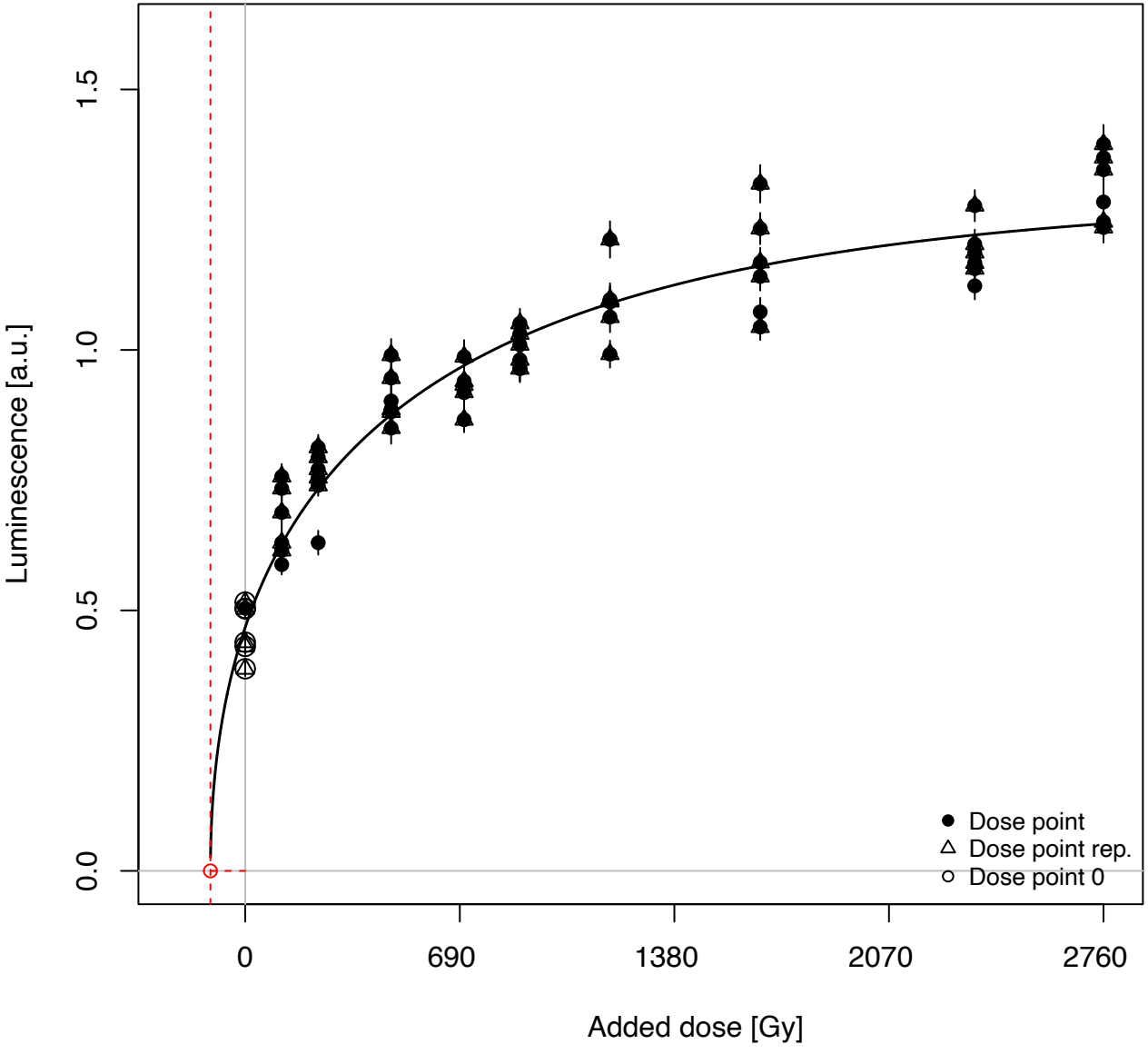

Figure
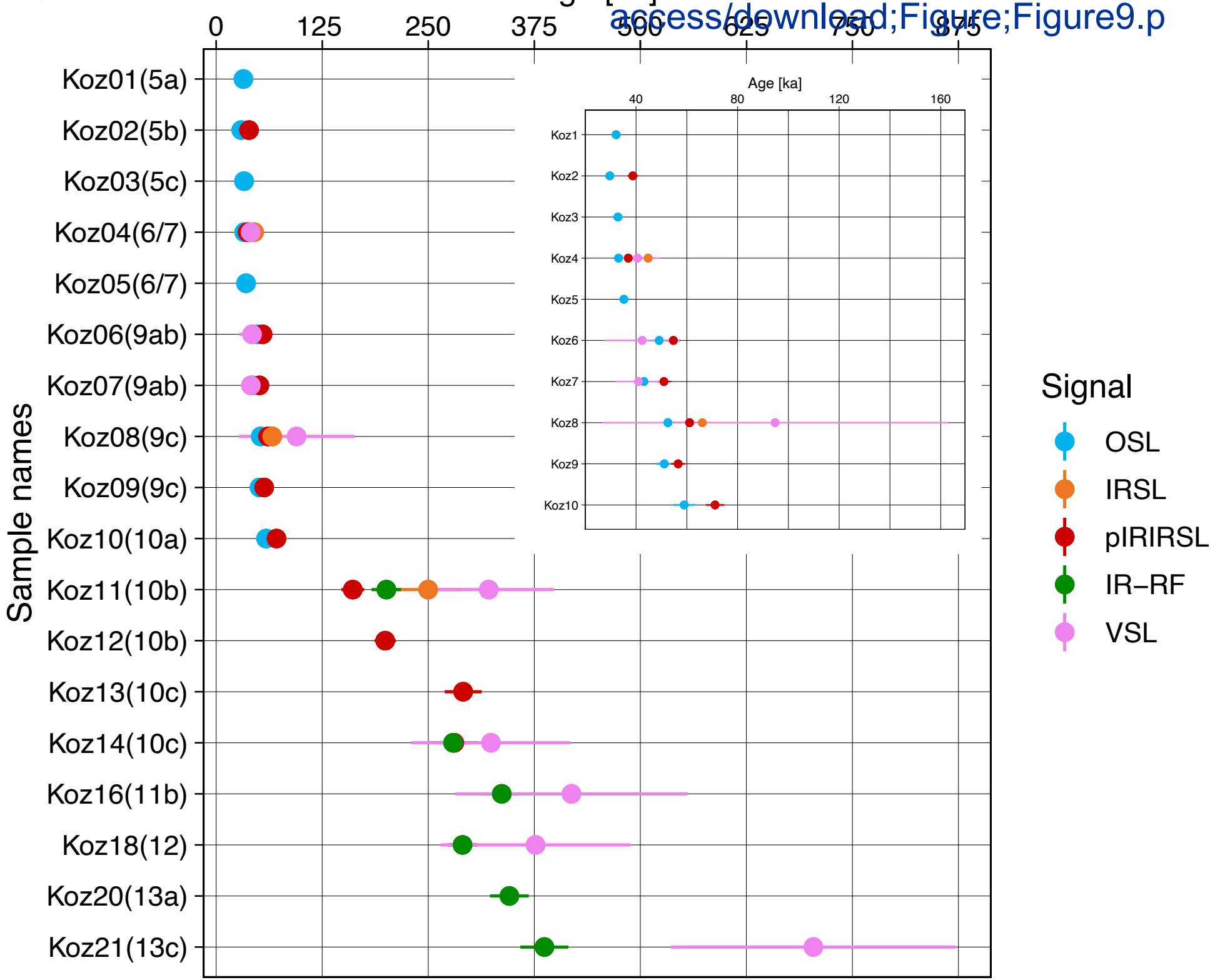
Click here to access/download;Figure;Figure9.p